

---

# Intrinsically Motivated Exploration for Automated Discovery of Patterns in Morphogenetic Systems

---

**Chris Reinke**  
Flowers Team, Inria  
Bordeaux, France  
chris.reinke@inria.fr

**Mayalen Etcheverry**  
Flowers Team, Inria  
Bordeaux, France  
mayalen.etccheverry@inria.fr

**Pierre-Yves Oudeyer**  
Flowers Team, Inria  
Bordeaux, France  
pierre-yves.oudeyer@inria.fr

## Abstract

Exploration is a cornerstone both for machine learning algorithms and for science in general to discover novel solutions, phenomena and behaviors. Intrinsically motivated goal exploration processes (IMGEPs) were shown to enable autonomous agents to efficiently explore the diversity of effects they can produce on their environment. With IMGEPs, agents self-define their own experiments by imagining goals, then try to achieve them by leveraging their past discoveries. Progressively they learn which goals are achievable. IMGEPs were shown to enable efficient discovery and learning of diverse repertoires of skills in high-dimensional robots. In this article, we show that the IMGEP framework can also be used in an entirely different application area: automated discovery of self-organized patterns in complex morphogenetic systems. We also introduce a new IMGEP algorithm where goal representations are learned online and incrementally (past approaches used precollected training data with batch learning). For experimentation, we use Lenia, a continuous game-of-life cellular automaton. We study how IMGEPs enable to discover a variety of complex self-organized visual patterns. We compare random search and goal exploration methods with hand-defined, pretrained and online learned goal spaces. The results show that goal exploration methods identify more diverse patterns compared to random explorations. Moreover, the online learned goal spaces allow to successfully discover interesting patterns similar to the ones manually identified by human experts. Our results exemplify the ability of IMGEPs to discover novel structures and patterns in complex systems. We are optimistic that their application will aid the understanding and discovery of new knowledge in various domains of science and engineering.

## 1 Introduction

Exploration is the process of searching new solutions for a problem or new information about a system. It is a cornerstone of many machine learning algorithms. For example, a robotic reinforcement learning agent may have to explore for discovering new objects and effects it can produce on them. Moreover, exploration is an important part for knowledge discovery in science and engineering. In order to understand or optimize a system, one must explore to discover what are its properties and behaviours.

---

Code and additional videos at <https://automated-discovery.github.io/>

Intrinsically motivated goal exploration processes (IMGEPs) have shown to be efficient exploration strategies for autonomous agents to discover and map the diversity of effects they can produce in their environment [3, 12, 26]. With IMGEPs, agents self-define their own experiments by imagining goals, then try to achieve them by leveraging their past discoveries (Fig. 1). Progressively they learn which goals are achievable and which are not. The goals are defined in a space of representations called *goal space*. It describes the important features of the direct observations. For a robot that interacts with objects the locations and properties of those objects could be such features [12]. With deep neural networks, the goal representations can be directly learned from raw pixel perception by training the latent layers of autoencoders with pre-collected data [26, 30].

So far, IMGEPs have been mainly used in the context of autonomous learning agents and robots. They enable an efficient exploration of diverse skill repertoires in high-dimensional robots [3, 12]. Nonetheless, their exploration capabilities are not constrained to this field and can be used in a variety of application scenarios. In this paper we exemplify their application for automating the discovery of complex patterns in high-dimensional complex systems such as studied in developmental (theoretical) biology, chemistry or physics. Based on our results, IMGEPs show a high potential to be efficient tools for helping scientists to discover and analyze novel high-dimensional self-organized structures in these complex systems. In a recent step in that direction, Grizou et al. [17] showed that IMGEPs are capable of making autonomously discoveries in a chemical system. However, the approach was based on a simple low-dimensional hand engineered goal space. In this paper we show that the full abilities of IMGEPs can be utilized for such environments by also learning in an unsupervised manner the representations that define the goal space. We show this ability on the example of discovering morphogenetic patterns in *Lenia* [6], a continuous game-of-life cellular automaton.

Moreover, we introduce with this paper a new IMGEP algorithm able to learn online the representations for its goal space. In previous IMGEP approaches, the goal representation either had to be defined by hand [12] or learned before the exploration with prerecorded data [30]. This required either expert knowledge about the system or existing data that might bias the exploration. The online learning approach can be directly applied without expert knowledge or preexisting data.

In summary, the paper provides the following new contributions:

- The application of IMGEPs in a new domain: The discovery of structures and patterns in high-dimensional complex systems with autonomous learning of goal representations.
- A novel online representation learning algorithm for IMGEPs that does not rely on expert knowledge or precollected data.

## 2 Related Work

*Intrinsically-motivated* learning [2, 3] is a family of computational models that autonomously organize an agents exploration curriculum in order to discover efficiently a maximally diverse set of outcomes the agent can produce in an unknown environment. The models are inspired from the way children self-develop a hierarchy of skills in order to make sense of the world. Intrinsically Motivated Goal Exploration Processes (IMGEPs) [3, 12] build upon those models. They are a family of curiosity-driven algorithms which have been developed to allow the exploration of high-dimensional complex real world systems. Population-based versions of these algorithms, which leverage episodic memory and hindsight learning, have shown to enable artificial agents, such as robots, to acquire diverse repertoires of skills [12, 37]. For example, they are able to bootstrap the exploration capacity for deep reinforcement learning problems with rare or deceptive rewards [8]. Recent work [26, 30] studies how to automatically learn the goal representations with the use of deep variational autoencoders. However, the training is done passively and in an early stage on a precollected set of available observations. A related family of algorithms to IMGEPs in evolutionary computation is novelty search [27] and quality-diversity algorithms [32], which can be formalized as special kind of population-based IMGEPs with a fixed random goal sampling policy.

Intrinsically motivated learning techniques have also been widely developed to handle exploration in reinforcement learning. Diverse approaches were studied ranging from estimating visitation counts [4], measures of empowerment [16], goal exploration approaches [11] with hindsight learning [1] and automated curriculum [9], or related concepts such as auxiliary tasks [36] and general value functions [40]. Recent approaches [29, 31] also introduced the usage of an online training of VAEs to learn the important features of a goal space similar to the methods in this paper. However, these approaches

focused on the problem of sequential decisions in MDPs (incurring a cost on sample efficiency). The approaches are orthogonal to the automated discovery framework considered here with independent experiments allowing the use of memory-based sampling efficient methods.

Active inquiry-based learning strategies have been used in biology [22, 23], chemistry [10] and astrophysics [35] to autonomously query which set of experiments to perform in order to improve the overall model of the system. These data-driven approaches considerably reduce the experimental costs but still require a database of representative experiments. Recently, machine learning algorithms [33, 34, 38] have been integrated into the experimental laboratory and often combined to the use of robotics and automation platforms [15, 20]. These methods open a brand new perspective to the way scientific experiments are conducted, but most of them rely on expert knowledge and optimize specific target properties. Rather than trying to find the optimal physico-chemical model from a database of collected experiments, we are interested to automatically discover a diversity of unseen patterns without requiring prior knowledge of the system.

We are using representation learning methods to identify autonomously goal spaces for IMGEPs. Representation learning aims at finding low-dimensional explanatory factors representing high-dimensional input data [5]. It is a key problem in a many areas in order to understand the underlying structure of complex observations. Deep *variational autoencoders* (VAE) [24] are one of the most popular approaches. Many state-of-the-art methods [7, 18, 19, 21, 25, 43] build on top of them using varying objectives and network architectures. See Tschannen et al. [41] for an in-depth review.

### 3 Method

This section describes intrinsically motivated goal exploration processes and the online learning approach for representations used as their goal spaces.

#### 3.1 Intrinsically Motivated Goal Exploration Processes

An IMGEP is a sequence of experiments that explore the parameters of a system by targeting self-generated goals (Fig. 1). It aims to maximize the diversity of observations from that system within a budget of  $N$  experiments.

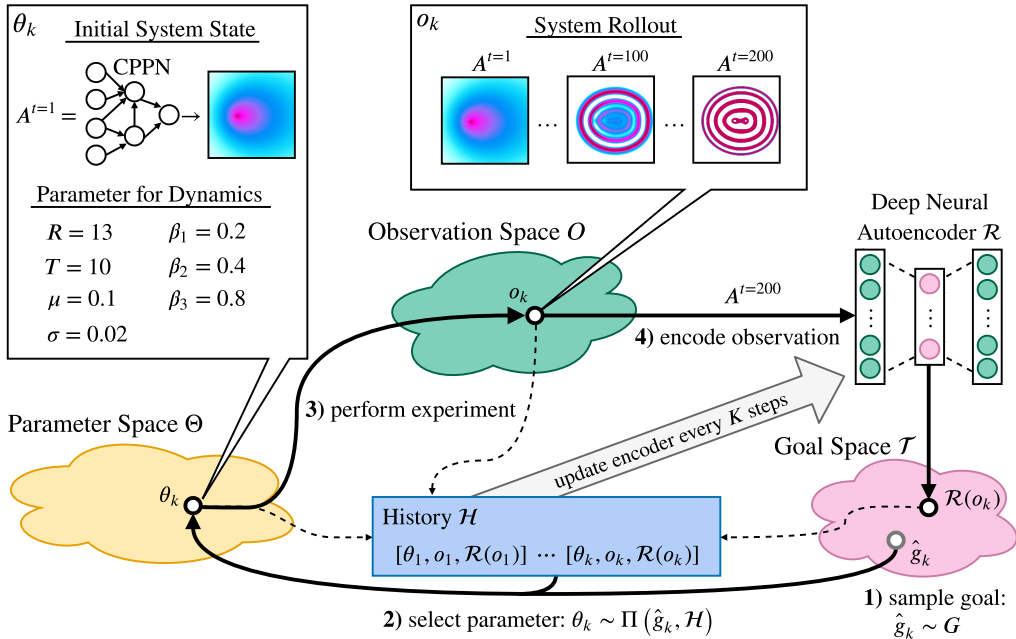


Figure 1: The intrinsically motivated goal exploration process (IMGEP) on the example of the IMGEP-OGI algorithm and Lenia as target system.

The systems are defined by three components. A parameter space  $\Theta$  corresponding to the controllable system parameters  $\theta$ . An observation space  $O$  where an observation  $o$  is a vector representing all the signals captured from the system. For this paper, the observations are a time series of images which depict the morphogenesis of activity patterns. Finally, an unknown environment dynamic  $D: \Theta \rightarrow O$  which maps parameters to observations.

To explore a system, an IMGEP defines a goal space  $\mathcal{T}$  that represents relevant features of its observations. For a robot that has to manipulate objects and observes them with a video camera, those features could be the object positions. From this goal space a goal  $g \sim G(\mathcal{H})$  is sampled by a goal sampling distribution. In the robot example this corresponds to a sampling of positions to which the robot should move the objects. Then, a parameter  $\theta$  is chosen that will be explored to reach goal  $g$ . The parameter is chosen according to a parameter sampling policy  $\Pi = \Pr(\theta; g, \mathcal{H})$ . Usually, the parameter sampling policy and in some cases the goal sampling distribution take into account previous explorations which are stored in a history  $\mathcal{H}$ . After a parameter is selected it is explored on the system and the outcome  $o$  observed. Based on the observation the actually reached goal is computed using an encoding function  $\hat{g} = \mathcal{R}(o)$ . The encoder is either hand-defined or in the case of our online approach learned via a variational autoencoder. The reached goal is together with its corresponding parameter and observation stored in a history  $\mathcal{H}$ . The exploration process is repeated until a certain number of steps  $N$  or another constraint is reached. Because the sampling of goals and parameters depend on a history of explored parameters, an initial set of  $N_{init}$  parameters are randomly sampled and explored before the intrinsically motivated goal exploration process starts.

Different goal and parameter sampling mechanisms can be used within this architecture [3, 13]. We chose for both basic approaches. Goals are sampled from a uniform distribution over the goal space. Parameters are chosen by selecting for a given goal the parameter from the history whose reached goal has the shortest distance in the goal space to the given goal. This parameter is then mutated by a random process.

### 3.2 Learning of Goal Spaces via Online Representation Learning

For IMGEPs the definition of the goal space  $\mathcal{T}$  and its corresponding encoder  $\mathcal{R}$  are a critical part, because they define which observations the process tries to identify from the target system. A straightforward choice to define a goal space is by selecting features manually, such as by using computer vision algorithms to detect the positions of objects from video images [12, 17]. A problematic point of this approach is its requirement of expert knowledge to select helpful features. Moreover, even experts might not know which features are important or how to formulate them for unknown or high-dimensional systems.

---

#### Algorithm 1: IMGEP-OGL

---

```

1 Initialize goal space encoder VAE  $\mathcal{R}$  with random weights
2 for  $i \leftarrow 1$  to  $N$  do
3   if  $i < N_{init}$  then                                     // Initial random iterations to populate  $\mathcal{H}$ 
4      $\theta \leftarrow \mathcal{U}(\Theta)$ 
5   else                                                     // Intrinsically motivated iterations
6     Sample a goal  $g \sim \mathcal{G}(\mathcal{H})$  based on space represented by  $\mathcal{R}$ 
7     Choose  $\theta \sim \Pi(g, \mathcal{H})$ 
8     Perform an experiment with  $\theta$  and observe  $o$ 
9     Encode reached goal  $\hat{g} = \mathcal{R}(o)$ 
10    Append  $(\theta, o, \hat{g})$  to the history  $\mathcal{H}$ 
11    if  $i \bmod K == 0$  then                                   // Periodically train the network
12      for  $E$  epochs do
13        Train  $\mathcal{R}$  on observations in  $\mathcal{H}$  with importance sampling
14      for  $(\theta, o, \hat{g}) \in \mathcal{H}$  do                           // Update the database of reached goals
15         $\mathcal{H}[\hat{g}] \leftarrow \mathcal{R}(o)$ 

```

---

A more elaborated approach is to learn goal space features by unsupervised representation learning. Representation learning is able to learn a mapping  $\mathcal{R}(o)$  from the raw sensor observations  $o$  to a compact latent vector  $\mathbf{z} \in \mathbb{R}^d$ . This latent mapping can be used as a goal space where a latent vector  $\mathbf{z} = g$  is interpreted as a goal.

Previous approaches already applied successfully the learning of goal spaces with variational autoencoders (VAE) [26, 30]. However, the goal spaces were learned before the start of the exploration from a prerecorded dataset of observations from the target system. During the exploration the learned representations were kept fixed. A problem with this pretraining approach is that training samples may be limited and often biased towards the initial knowledge about the system.

In this paper we attempt to address this problem by continuously adapting the learned representation to the observations that are encountered during the exploration process. We believe it is crucial to learn the representation of features for new and unseen observations to further enable the discovery of a diversity of similar observations. To address this challenge, we propose an online goal space learning IMGEP (IMGEP-OGL), which learns the goal space in an incremental manner during the exploration process (Algorithm 1). We evaluated different variants of VAEs for the representation learning part of the algorithm. The Supplementary Material provides further details about the different VAE variants.

The training procedure of the VAE is integrated in the goal sampling exploration process by first initializing the VAE with random weights. The VAE network is then trained every  $K$  explorations for  $E$  epochs on the observation collected in the history  $\mathcal{H}$ . Importance sampling is used to give more weight to recently discovered patterns.

## 4 Experiments

The usefulness of IMGEPs for the discovery of novel patterns in complex system was evaluated on the Lenia system. The following sections introduce Lenia, the different algorithms that were compared and the experimental procedure. Please refer to the Supplementary Materials for further details about the procedure and additional algorithm variants that have been compared.

### 4.1 Target System: Lenia

Lenia [6] is a continuous cellular automaton [42] similar to Conway’s Game of Life [14]. Game-of-life systems have been used many times as abstract models for theoretical understanding of how self-organized structures, including solitons, may form in natural morphogenetic systems. Lenia, in particular, represents a high-dimensional complex dynamical system where diverse visual structures can self-organize and yet are hard to find by manual exploration. It is therefore well suited to test the performance of exploration algorithms for unknown and complex systems.

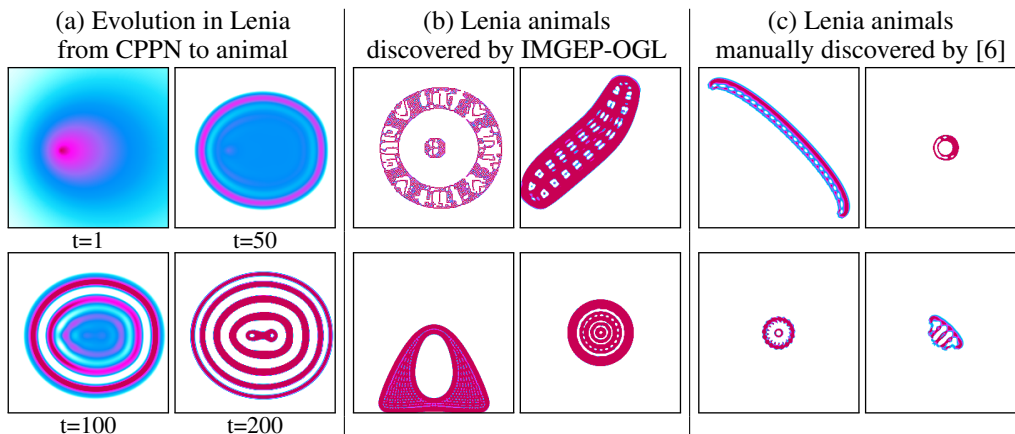


Figure 2: Example patterns produced by the Lenia system. Illustration of the dynamical morphing from an initial CPPN image to an animal (a). The automated discovery (b) is able to find similar complex animals as a human-expert manual search (c) by [6].

Lenia consists of a two-dimensional grid of cells  $A \in [0, 1]^{256 \times 256}$  where the state of each cell is a real-valued scalar activity  $A^t(x) \in [0, 1]$ . The state of cells evolves over discrete time steps  $t$  (Fig. 2, a). The activity change is computed by integrating the activity of neighbouring cells. Lenia’s behavior is controlled by its initial pattern  $A^{t=1}$  and several settings that control the dynamics of the activity change ( $R, T, \mu, \sigma, \beta_1, \beta_2, \beta_3$ ). Please see the Supplementary Material for details about Lenia.

Lenia can be understood as a morphogenetic system where the parameters represent the genes of a developmental process. They control into which final activity pattern the initial pattern morphs. Lenia can produce diverse patterns with different dynamics such as stable, non-stable or chaotic patterns. Most interesting, patterns that resemble microscopic animals can be produced (Fig. 2, b, c). We use Lenia to study if IMGEPs can autonomously discover such patterns.

We implemented different pattern classifiers to analyze the exploration results. We differentiate between dead and alive patterns. A pattern is dead if the activity of all cells are either 0 or 1. Alive patterns are separated into animals and non-animals. Animals are a connected areas of positive activity which are finite, i.e. which do not infinitely cross several borders. All other patterns are non-animals whose activity usually spreads over the whole state space.

## 4.2 Algorithms

The exploration behaviors of different IMGEP algorithms were evaluated and compared to a random exploration. The IMGEP variants differ in their way how the goal space is defined or learned. We tested for each algorithm class several variants and selected the optimal ones. Please see the Supplementary Material for more information about the different variants.

**Random exploration:** The IMGEP variants were compared to a random exploration that sampled randomly for each of the  $N$  exploration iterations the parameters  $\theta$  including the initial state  $A^{t=1}$ .

**IMGEP-HGS - Goal exploration with a hand-defined goal space:** The first IMGEP uses a hand-defined goal space that is composed of 5 features. Each feature measures a certain property of the final pattern  $A^{t=200}$  that emerged in Lenia: 1) the sum over the activity of all cells, 2) the number of activated cells, 3) the density of the activity center, 4) an asymmetry measure of the pattern and 5) a distribution measure of the pattern.

**IMGEP-PGL - Goal exploration with a pretrained goal space:** For this IMGEP variant the goal space was learned with a VAE approach on training data before the exploration process started. The training set consisted of 558 Lenia patterns. Half of the patterns were animals that have been manually identified by [6]. The other half were randomly initialized patterns that were created with the same procedure as described in Section 4.3.

**IMGEP-UGL - Goal exploration with online learning of the goal space:** The final algorithm is the new online variant for IMGEPs (Algorithm 1).

## 4.3 Experimental Procedure

For each algorithm 10 repetitions of the exploration experiment were conducted to measure their average performance. Each experiment consisted of  $N = 5000$  exploration iterations. For IMGEP variants the first  $N_{\text{init}} = 1000$  iterations were random explorations to populate their histories  $\mathcal{H}$ . For all algorithms an identical initial set of random explorations was used to allow a better comparison between them. For the following 4000 iterations each IMGEP approach sampled a goal  $g$  via an uniform distribution over its goal space. Then, the parameter  $\theta_k$  from a previous exploration in  $\mathcal{H}$  was selected whose reached goal  $\hat{g}_k$  had the minimum euclidean distance to the current goal  $g$  within the goal space. This parameter was then mutated by a random process to generate the parameter  $\theta$  that was explored.

The parameters consisted of a compositional pattern producing network (CPPN) [39] that generates the initial state  $A^{t=1}$  for Lenia and the settings defining Lenia’s dynamics:  $\theta = [\text{CPPN} \rightarrow A^{t=1}, R, T, \mu, \sigma, \beta_1, \beta_2, \beta_3]$ . CPPNs are recurrent neural networks that were originally used to generate and evolve gray scale images, but that can be similarly used to generate Lenia patterns. The networks are initialized and mutated by a random process that defines their structure and connection weights as done in [39]. The random initialization of the other Lenia settings was done by an uniform distribution and their mutation by a Gaussian distribution around the original values.

The meta parameters to initialize and mutate the parameters were the same for all algorithms (see the Supplementary Material). They were manually chosen without optimizing them for a specific algorithm. The parameters of the CPPN networks were set to initialize and mutate networks that generate similar patterns as in [39].

## 5 Results

We compared random explorations and IMGEP algorithms on their ability to identify a set of Lenia patterns with a high diversity. Diversity is measured in an analytic behavior space constructed by hand-defined and learned features. Furthermore, we compared the goal spaces of hand-defined and learned IMGEP variants.

### 5.1 Diversity of Explored Lenia Patterns

Diversity is measured by the spread of the exploration in an *analytic behavior space* defined by 13 features. We constructed this space because the observation space  $O$ , i.e. the final Lenia patterns  $A^{t=200}$ , are too high-dimensional. The features of the new space are: 1) the sum over the activity of all cells, 2) the number of activated cells, 3) the density of the activity center, 4) an asymmetry measure of the pattern, 5) a distribution measure of the pattern and 6-13) a latent representation of the pattern by a VAE. The VAE was trained on a dataset of Lenia patterns that were identified during all performed experiments. Please see the Supplementary Material for details.

For each experiment all explored patterns were projected into the analytic behavior space. To measure the diversity of the found solutions we used a simple measure of the area that the exploration covered in the analytic behavior space. The measure discretizes the analytic behavior space into bins of equal size by splitting each dimension into 7 sections resulting in  $7^{13}$  bins. The number of bins in which at least one explored entity falls is used as a measure for diversity.

We also measured the diversity in the space of parameters  $\Theta$  by constructing an *analytic parameter space*. The 15 features of this space consisted of Lenia’s parameters  $(R, T, \mu, \sigma, \beta_1, \beta_2, \beta_3)$  and

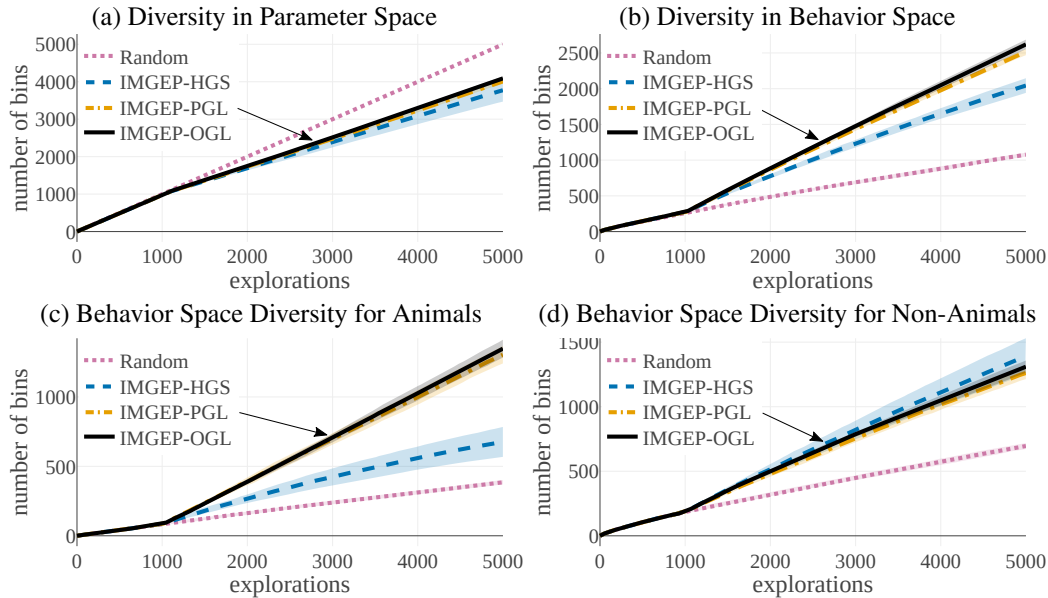


Figure 3: (a) Although random explorations reach the highest diversity in the analytic parameter space, (b) IMGEPs reach a higher diversity in the analytic behavior space. They discover a more diverse set of Lenia patterns. (c) IMGEPs with a learned goal space discovered a larger diversity of animals compared to the IMGEP with a hand-defined goal space. (d) For non-animals the hand-defined goal space discovered the highest diversity. Depicted is the average diversity ( $n = 10$ ) with the standard deviation as shaded area (for some not visible because it is too small).

the latent representation of a VAE. The VAE was trained on a dataset of initial Lenia states ( $A^{t=1}$ ) that were used during the experiments. Also for this diversity 7 bins per dimension were used to discretize the space.

Comparing the diversity between the analytic parameter and behavior space reveals the advantage of IMGEPs over random explorations (Fig. 3, a, b). Although random explorations have reached the highest diversity in the space of parameters, they are outperformed in terms of diversity by the IMGEP approaches in the analytic behavior space. Thus, the IMGEP approaches are better in the actual objective of our exploration, finding a diverse set of Lenia patterns.

Both IMGEPs (PGL and OGL) with learned goal spaces reached a higher diversity over all patterns than the one with a hand-defined goal space (HGS) (Fig. 3, b). Nonetheless, this is not the case for certain subgroups of patterns. In the case of comparing the diversity only over explored animals (Fig. 3, c) the new online approach IMGEP-OGL is finding the highest diversity of animals. It is closely followed by the pretrained IMGEP-PGL approach. The hand-defined goal space approach IMGEP-HGS can identify a diversity of 50% compared to IMGEP-OGL. Random explorations find only less than 30% compared to IMGEP-OGL. In the case of diversity over non-animal patterns (Fig. 3, d) the IMGEP-HGS reached the highest diversity followed by the IMGEP-OGL and IMGEP-PGL. Random explorations reached the lowest diversity. These results show that the goal-space has a critical influence on the type of patterns that are identified.

## 5.2 Differences in Goal Spaces

We analyzed the goal spaces of the different IMGEP variants to understand their behavior by visualizing their reached goals in a two-dimensional space. T-SNE [28] was used to reduce the high-dimensional goal spaces. It puts points that were nearby in the high-dimensional space also close to each other in the two-dimensional visualization.

The goal spaces of IMGEP-HGS and IMGEP-OGL show strong differences between each other (Fig. 4) which we believe explain their different abilities to find either a high diversity of non-animals or animals (Fig. 3, c, d). The goal space of the IMGEP-HGS shows large areas and several clusters for non-animal patterns (Fig. 4, a). Animals form only few and nearby clusters. Thus, the hand-defined features seem poor to discriminate and describe animal patterns in Lenia. As a consequence, when goals are uniformly sampled within this goal space during the exploration process, then more goals are generated in regions that describe non-animals. This can explain why IMGEP-HGS explored a high diversity of non-animal patterns but only a low diversity of animal patterns.

In contrast, features learned by IMGEP-OGL capture better factors that differentiate animal patterns. This is indicated by the several clusters of animals that span a wide area in its goal space (Fig. 4, b). We attribute this effect to the difficulty of VAEs to capture sharp details [44]. They therefore represent mainly the general form of the patterns but not their fine-grained structures. Animals differ often in their form whereas non-animals occupy often the whole cell grid and differ in their fine-grained details. The goal spaces learned by VAEs seem therefore better suited for exploring diverse sets of animal patterns.

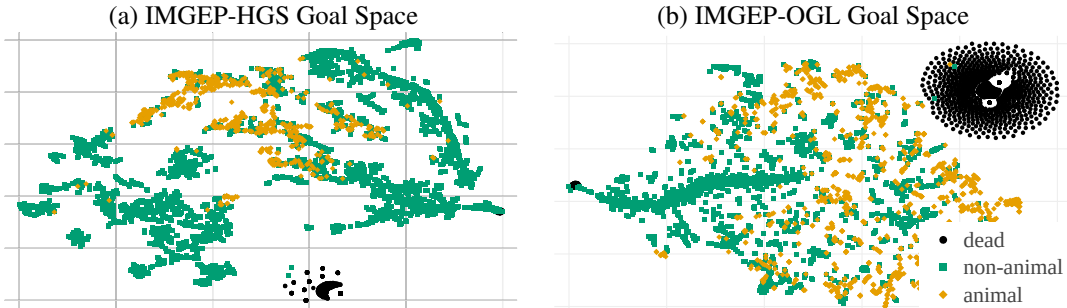


Figure 4: (a) Hand-defined and (b) learned goal spaces have major differences shown here by a t-SNE visualization. The different size of areas covered by animals or non-animals can explain the differences in their resulting diversity between the algorithms (Fig. 3).

## 6 Conclusion

We presented in this paper the application of intrinsically motivated exploration via IMGEPs towards a new and exciting application area: the discovery of patterns and structures in complex systems. All evaluated IMGEP variants were able to discover a diverse set of patterns for Lenia, a cellular automaton, by directly exploring its high-dimensional parameters and observing its high-dimensional output patterns. We could demonstrate that goal spaces for such systems can be successfully learned via deep VAEs which allow the identification of animal-like patterns similar to those identified by human experts (Fig. 2). Moreover, our new approach of learning goal spaces online via data collected during the exploration process could outperform a pretrained and fixed goal space in terms of identifying a diverse set of animal-like patterns.

We believe that IMGEPs are able to facilitate the study of similar complex and high-dimensional systems in different fields of engineering and science such as physics and chemistry. IMGEPs allow to explore and discover efficiently interesting behaviors and patterns of unknown systems. This knowledge helps to understand the systems better or to find new solutions for problems in them.

### Acknowledgments

We thank Bert Wang-Chak Chan for his helpful discussions about the Lenia system and Jonathan Grizou for his comments on the visualization of our results.

### References

- [1] Marcin Andrychowicz, Filip Wolski, Alex Ray, Jonas Schneider, Rachel Fong, Peter Welinder, Bob McGrew, Josh Tobin, OpenAI Pieter Abbeel, and Wojciech Zaremba. Hindsight experience replay. In *Advances in Neural Information Processing Systems*, pages 5048–5058, 2017.
- [2] Gianluca Baldassarre and Marco Mirolli. *Intrinsically motivated learning in natural and artificial systems*. Springer, 2013.
- [3] Adrien Baranes and Pierre-Yves Oudeyer. Active learning of inverse models with intrinsically motivated goal exploration in robots. *Robotics and Autonomous Systems*, 61(1):49–73, 2013.
- [4] Marc Bellemare, Sriram Srinivasan, Georg Ostrovski, Tom Schaul, David Saxton, and Remi Munos. Unifying count-based exploration and intrinsic motivation. In *Advances in Neural Information Processing Systems*, pages 1471–1479, 2016.
- [5] Yoshua Bengio, Aaron Courville, and Pascal Vincent. Representation learning: A review and new perspectives. *IEEE transactions on pattern analysis and machine intelligence*, 35(8):1798–1828, 2013.
- [6] Bert Wang-Chak Chan. Lenia-biology of artificial life. *arXiv preprint arXiv:1812.05433*, 2018.
- [7] Tian Qi Chen, Xuechen Li, Roger B Grosse, and David K Duvenaud. Isolating sources of disentanglement in variational autoencoders. In *Advances in Neural Information Processing Systems*, pages 2610–2620, 2018.
- [8] Cédric Colas, Olivier Sigaud, and Pierre-Yves Oudeyer. Gep-pg: Decoupling exploration and exploitation in deep reinforcement learning algorithms. *arXiv preprint arXiv:1802.05054*, 2018.
- [9] Cédric Colas, Olivier Sigaud, and Pierre-Yves Oudeyer. Curious: Intrinsically motivated multi-task, multi-goal reinforcement learning. In *International Conference on Machine Learning (ICML)*, 2019.
- [10] Vasilios Duros, Jonathan Grizou, Weimin Xuan, Zied Hosni, De-Liang Long, Haralampos N Miras, and Leroy Cronin. Human versus robots in the discovery and crystallization of gigantic polyoxometalates. *Angewandte Chemie*, 129(36):10955–10960, 2017.
- [11] Carlos Florensa, David Held, Markus Wulfmeier, Michael Zhang, and Pieter Abbeel. Reverse curriculum generation for reinforcement learning. *arXiv preprint arXiv:1707.05300*, 2017.
- [12] Sébastien Forestier, Yoan Mollard, and Pierre-Yves Oudeyer. Intrinsically motivated goal exploration processes with automatic curriculum learning. *arXiv preprint arXiv:1708.02190*, 2017.

- [13] Sébastien Forestier and Pierre-Yves Oudeyer. Modular active curiosity-driven discovery of tool use. In *2016 IEEE/RSJ International Conference on Intelligent Robots and Systems (IROS)*, pages 3965–3972. IEEE, 2016.
- [14] Martin Gardener. Mathematical games: The fantastic combinations of john conway’s new solitaire game" life,". *Scientific American*, 223:120–123, 1970.
- [15] Jarosław M Granda, Liva Donina, Vincenza Dragone, De-Liang Long, and Leroy Cronin. Controlling an organic synthesis robot with machine learning to search for new reactivity. *Nature*, 559(7714):377, 2018.
- [16] Karol Gregor, Danilo Jimenez Rezende, and Daan Wierstra. Variational intrinsic control. *arXiv preprint arXiv:1611.07507*, 2016.
- [17] Jonathan Grizou, Laurie J Points, Abhishek Sharma, and Leroy Cronin. Exploration of self-propelling droplets using a curiosity driven robotic assistant. *arXiv preprint arXiv:1904.12635*, 2019.
- [18] Ishaan Gulrajani, Kundan Kumar, Faruk Ahmed, Adrien Ali Taiga, Francesco Visin, David Vazquez, and Aaron Courville. Pixelvae: A latent variable model for natural images. *arXiv preprint arXiv:1611.05013*, 2016.
- [19] Irina Higgins, Loic Matthey, Arka Pal, Christopher Burgess, Xavier Glorot, Matthew Botvinick, Shakir Mohamed, and Alexander Lerchner. beta-vae: Learning basic visual concepts with a constrained variational framework. In *International Conference on Learning Representations*, volume 3, 2017.
- [20] Claudia Houben and Alexei A Lapkin. Automatic discovery and optimization of chemical processes. *Current opinion in chemical engineering*, 9:1–7, 2015.
- [21] Hyunjik Kim and Andriy Mnih. Disentangling by factorising. *arXiv preprint arXiv:1802.05983*, 2018.
- [22] Ross D King, Jem Rowland, Stephen G Oliver, Michael Young, Wayne Aubrey, Emma Byrne, Maria Liakata, Magdalena Markham, Pinar Pir, Larisa N Soldatova, et al. The automation of science. *Science*, 324(5923):85–89, 2009.
- [23] Ross D King, Kenneth E Whelan, Ffion M Jones, Philip GK Reiser, Christopher H Bryant, Stephen H Muggleton, Douglas B Kell, and Stephen G Oliver. Functional genomic hypothesis generation and experimentation by a robot scientist. *Nature*, 427(6971):247, 2004.
- [24] Diederik P Kingma and Max Welling. Auto-encoding variational bayes. *arXiv preprint arXiv:1312.6114*, 2013.
- [25] Abhishek Kumar, Prasanna Sattigeri, and Avinash Balakrishnan. Variational inference of disentangled latent concepts from unlabeled observations. *arXiv preprint arXiv:1711.00848*, 2017.
- [26] Adrien Laversanne-Finot, Alexandre Pere, and Pierre-Yves Oudeyer. Curiosity driven exploration of learned disentangled goal spaces. In Aude Billard, Anca Dragan, Jan Peters, and Jun Morimoto, editors, *Proceedings of The 2nd Conference on Robot Learning*, volume 87 of *Proceedings of Machine Learning Research*, pages 487–504. PMLR, 29–31 Oct 2018.
- [27] Joel Lehman and Kenneth O Stanley. Exploiting open-endedness to solve problems through the search for novelty. In *ALIFE*, pages 329–336, 2008.
- [28] Laurens van der Maaten and Geoffrey Hinton. Visualizing data using t-sne. *Journal of machine learning research*, 9(Nov):2579–2605, 2008.
- [29] Ashvin V Nair, Vitchyr Pong, Murtaza Dalal, Shikhar Bahl, Steven Lin, and Sergey Levine. Visual reinforcement learning with imagined goals. In *Advances in Neural Information Processing Systems*, pages 9191–9200, 2018.
- [30] Alexandre Péré, Sébastien Forestier, Olivier Sigaud, and Pierre-Yves Oudeyer. Unsupervised Learning of Goal Spaces for Intrinsically Motivated Goal Exploration. In *ICLR2018 - 6th International Conference on Learning Representations*, Vancouver, Canada, April 2018.
- [31] Vitchyr H Pong, Murtaza Dalal, Steven Lin, Ashvin Nair, Shikhar Bahl, and Sergey Levine. Skew-fit: State-covering self-supervised reinforcement learning. *arXiv preprint arXiv:1903.03698*, 2019.

- [32] Justin K Pugh, Lisa B Soros, and Kenneth O Stanley. Quality diversity: A new frontier for evolutionary computation. *Frontiers in Robotics and AI*, 3:40, 2016.
- [33] Paul Raccuglia, Katherine C Elbert, Philip DF Adler, Casey Falk, Malia B Wenny, Aurelio Mollo, Matthias Zeller, Sorelle A Friedler, Joshua Schrier, and Alexander J Norquist. Machine-learning-assisted materials discovery using failed experiments. *Nature*, 533(7601):73, 2016.
- [34] Brandon J Reizman, Yi-Ming Wang, Stephen L Buchwald, and Klavs F Jensen. Suzuki–miyaura cross-coupling optimization enabled by automated feedback. *Reaction chemistry & engineering*, 1(6):658–666, 2016.
- [35] Joseph W Richards, Dan L Starr, Henrik Brink, Adam A Miller, Joshua S Bloom, Nathaniel R Butler, J Berian James, James P Long, and John Rice. Active learning to overcome sample selection bias: application to photometric variable star classification. *The Astrophysical Journal*, 744(2):192, 2011.
- [36] Martin Riedmiller, Roland Hafner, Thomas Lampe, Michael Neunert, Jonas Degraeve, Tom Van de Wiele, Volodymyr Mnih, Nicolas Heess, and Jost Tobias Springenberg. Learning by playing-solving sparse reward tasks from scratch. *arXiv preprint arXiv:1802.10567*, 2018.
- [37] Matthias Rolf, Jochen J Steil, and Michael Gienger. Goal babbling permits direct learning of inverse kinematics. *IEEE Transactions on Autonomous Mental Development*, 2(3):216–229, 2010.
- [38] Artur M Schweidtmann, Adam D Clayton, Nicholas Holmes, Eric Bradford, Richard A Bourne, and Alexei A Lapkin. Machine learning meets continuous flow chemistry: Automated optimization towards the pareto front of multiple objectives. *Chemical Engineering Journal*, 352:277–282, 2018.
- [39] Kenneth O Stanley. Exploiting regularity without development. In *Proceedings of the AAAI Fall Symposium on Developmental Systems*, page 37. AAAI Press Menlo Park, CA, 2006.
- [40] Richard S Sutton, Joseph Modayil, Michael Delp, Thomas Degris, Patrick M Pilarski, Adam White, and Doina Precup. Horde: A scalable real-time architecture for learning knowledge from unsupervised sensorimotor interaction. In *The 10th International Conference on Autonomous Agents and Multiagent Systems-Volume 2*, pages 761–768. International Foundation for Autonomous Agents and Multiagent Systems, 2011.
- [41] Michael Tschannen, Olivier Bachem, and Mario Lucic. Recent advances in autoencoder-based representation learning. *arXiv preprint arXiv:1812.05069*, 2018.
- [42] Stephen Wolfram. Statistical mechanics of cellular automata. *Reviews of modern physics*, 55(3):601, 1983.
- [43] Shengjia Zhao, Jiaming Song, and Stefano Ermon. Infovae: Information maximizing variational autoencoders. *arXiv preprint arXiv:1706.02262*, 2017.
- [44] Shengjia Zhao, Jiaming Song, and Stefano Ermon. Towards deeper understanding of variational autoencoding models. *arXiv preprint arXiv:1702.08658*, 2017.

---

# Supplementary Material for "Intrinsically Motivated Exploration for Automated Discovery of Patterns in Morphogenetic Systems"

---

**Chris Reinke**  
Flowers Team, Inria  
Bordeaux, France  
chris.reinke@inria.fr

**Mayalen Etcheverry**  
Flowers Team, Inria  
Bordeaux, France  
mayalen.etccheverry@inria.fr

**Pierre-Yves Oudeyer**  
Flowers Team, Inria  
Bordeaux, France  
pierre-yves.oudeyer@inria.fr

## Overview

The Supplementary Material for the paper "Intrinsically Motivated Exploration for Automated Discovery of Patterns in Morphogenetic Systems" provides implementation details and additional results. Section 1 introduces the target system of all experiments, Lenia, in more detail. The sampling procedure for the parameters that control Lenia are described in Section 2. Section 3 describes in more detail the diversity measure used to compare algorithms and the definition of the analytic parameter and behavior space in which it is measured. Afterwards, results for one additional random exploration and several variations of IMGEPs with hand-defined goal spaces are provided in Section 4. Section 5 provides results for different VAE variants used to learn goal spaces for IMGEPs. Finally, Section 6 lists additional results for the experiments that were omitted in the main paper.

## Contents

<b>1</b>	<b>Target System: Lenia</b>	<b>3</b>
1.1	Implementation Details and Parameters . . . . .	3
1.2	Classifier . . . . .	3
1.3	Statistical Measures for Lenia Patterns . . . . .	6
<b>2</b>	<b>Sampling of Parameters for Lenia</b>	<b>8</b>
2.1	Sampling of Start Patterns for Lenia via CPPNs . . . . .	8
2.2	Sampling of Lenia’s Dynamic Parameters . . . . .	11
<b>3</b>	<b>Measurement of Diversity in the Analytic Parameter and Behavior Space</b>	<b>12</b>
3.1	Diversity Measure . . . . .	12
3.2	Analytic Parameter Space . . . . .	12
3.3	Analytic Behavior Space . . . . .	12
<b>4</b>	<b>Random Exploration and IMGEPs with Hand-Defined Goal Spaces</b>	<b>16</b>
4.1	Random Explorations . . . . .	16
4.2	IMGEPs with Hand-Defined Goal Spaces . . . . .	16
4.3	Results . . . . .	16
<b>5</b>	<b>IMGEPs with Learned Goal Spaces via Deep Variational Autoencoders</b>	<b>19</b>
5.1	VAE Variants . . . . .	19
5.2	Implementation Details . . . . .	20
5.3	Results . . . . .	21
5.3.1	Diversity . . . . .	22
5.3.2	VAE Pattern Reconstruction . . . . .	22
<b>6</b>	<b>Additional Results</b>	<b>26</b>
6.1	Number of Identified Patterns . . . . .	26
6.2	Dependence of the Diversity Measure on the Number of Bins per Dimension . . . . .	27
6.3	Dimension Reduction of the Analytic Parameter and Behavior Space . . . . .	27
6.4	Identified Patterns . . . . .	29
6.5	Visualization of Goal Spaces . . . . .	29

# 1 Target System: Lenia

Lenia was used as the target system for all exploration experiments. The following section describes Lenia and the parameters to control its behavior in detail. It is followed by a description of the classifiers used to categorize dead, animal and non-animal Lenia patterns. Finally, statistical measures about the patterns are introduced which were used to define goal and analytic spaces.

## 1.1 Implementation Details and Parameters

Lenia [2] is a cellular automaton [18]. It consists of a two-dimensional grid of cells  $A \in [0, 1]^{L \times L}$  with  $L = 256$  for all experiments. The cell grid is similar to the surface of a ball. Cells on the north border are neighbors to the south border cells. The east and west border are also connected. The state of each cell is a real-valued scalar activity  $A(x) \in [0, 1]$ . The states of cells  $A^t$  evolve over discrete time steps  $t = [1, \dots, M]$  with  $M = 200$  for all experiments. The activity change of a cell is computed by integrating the previous activity of its neighbouring cells:

$$A^{t+1}(x) = [A^t(x) + \Delta t G(K * A^t(x))]_0^1,$$

where  $G$  is the *growth mapping*,  $K$  is the *kernel*,  $\Delta t = \frac{1}{T}$  with  $T \in \mathbb{N}$  is the *time step* and  $[n]_b^a = \min(\max(n, a), b)$  is the clip function. For all experiments an exponential growth mapping was used:

$$G(u; \mu, \sigma) = 2 \exp\left(-\frac{(u - \mu)^2}{2\sigma^2}\right) - 1,$$

with  $\mu \in \mathbb{R}$  and  $\sigma \in \mathbb{R}$  being parameters that control its shape.

The kernel integrates the activity of the current cell  $x$  and its neighbours by a convolution with a *kernel function*  $K(n)$ :

$$K * A^t(x) = \sum_{n \in \mathcal{N}(x)} K(n) A^t(x + n) \Delta x^2, \quad (1)$$

where  $\mathcal{N}$  is the *neighborhood* around the cell  $x$  and  $\Delta x = \frac{1}{R}$  with  $R \in \mathbb{N}$  is the site distance. The neighborhood is defined by a circle around  $x$  with radius  $R$ :  $\mathcal{N}(x) = \{y : \|x - y\|_2 \leq R\}$ . The kernel is constructed by a *kernel core* function  $K_C : [0, 1] \mapsto [0, 1]$  and a *kernel shell* function  $K_S : [0, 1] \mapsto [0, 1]$ . The kernel core creates a ring around the center coordinate and is defined by an exponential:

$$K_C(r) = \exp\left(\alpha - \frac{\alpha}{4r(1-r)}\right) \text{ with } \alpha = 4.$$

The kernel shell  $K_S$  takes a vector parameter  $\beta = (\beta_1, \beta_2, \beta_3) \in [0, 1]^3$  and copies the kernel core into concentric rings. The rings are of equal thickness with peak heights  $\beta_i$ :

$$K_S(r; \beta) = \beta_{\lfloor Br \rfloor} K_C(Br \bmod 1).$$

Finally, the kernel is normalized:

$$K(n) = \frac{K_S(\|n\|_2)}{|K_S|}.$$

In total 8 parameters  $\theta = \{A^{t=1}, R, T, \mu, \sigma, \beta_1, \beta_2, \beta_3\}$  controlled the behavior of Lenia for all experiments.  $A^{t=1}$  is the starting pattern of the system.  $R$  is the radius of the circle around a cell  $x$  whose enclosed cells influence the activity of  $x$ .  $T$  controls the growth strength update per time step. The growth mapping is controlled by  $\mu$  and  $\sigma$ . The form of the kernel function is controlled by  $\beta_1, \beta_2, \beta_3$ .

We based our Python implementation of Lenia on the code provided by <https://github.com/Chakazul/Lenia>.

## 1.2 Classifier

We categorized 3 types of patterns that are observed in Lenia. The categories were used to analyze if the exploration algorithms showed differences in their exploration behaviors by identifying different types of patterns. The 3 categories are dead, animals and non-animals. For each class is a classifier

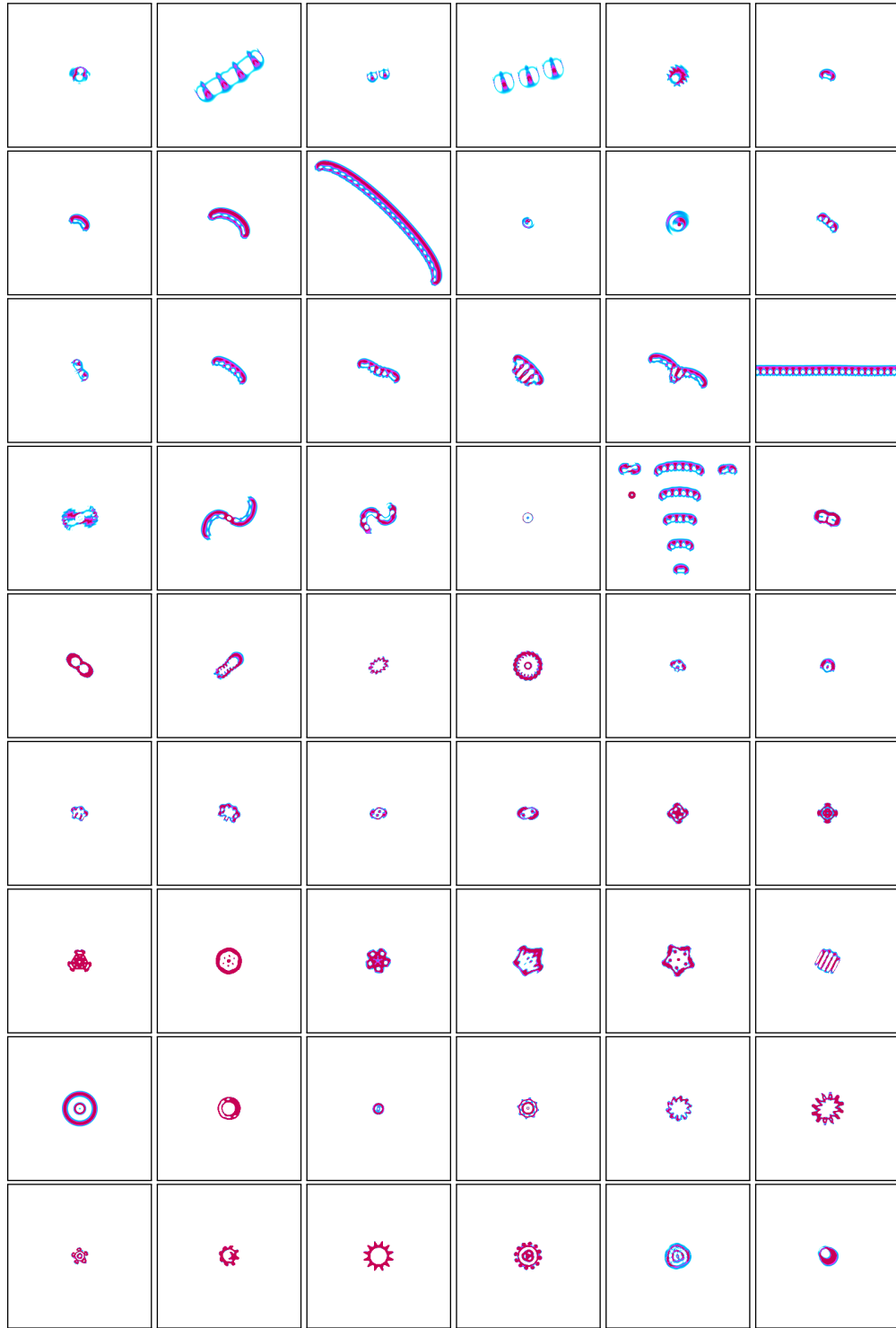


Figure 1: Patterns identified by a human-expert [2].

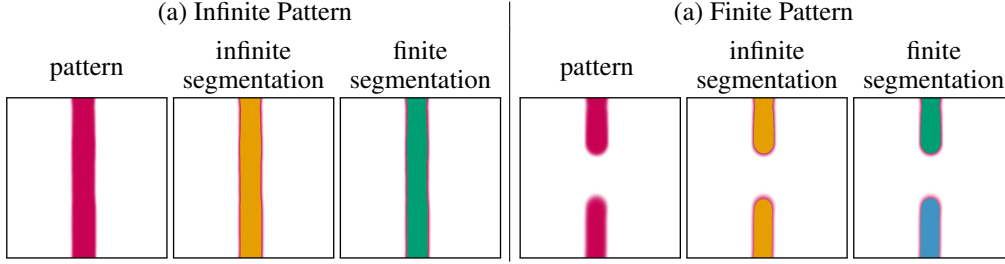


Figure 2: Classification of Lenia patterns into finite and infinite patterns. Infinite patterns form loop between the image borders which are identified if a segment is connected between two borders in the infinite and finite segmentation. Finite patterns form no loops. They have connected segments between borders in the infinite but not finite segmentation. Segments are colored in yellow, green and blue.

defined. The classifiers only classify the final pattern in which the Lenia system morphs after  $M = 200$  time steps.

**Dead Classifier:** For dead patterns is the activity of all cells either 0 or 1 in the last time step.

**Animal Classifier:** The final Lenia pattern is classified as an animal if it is a *finite* and *connected* pattern of activity. Cells  $x, y$  are connected as a pattern if both are active ( $A(x) \geq 0.1$  and  $A(y) \geq 0.1$ ) and if they influence each other. Cells influence each other when they are within their radius of the kernel  $K$  as defined by the parameter  $R$  (Eq. 1).

Furthermore, the connected pattern must be finite. In Lenia finite and infinite patterns can be differentiated because the opposite borders of Lenia's cell grid are connected, so that the space is similar to a ball surface. Thus, a pattern can loop around this surface making it infinite. We identify infinite patterns by the following approach. First, all connected patterns are identified for the case of assuming an infinite grid cell, i.e. opposite grid cell borders are connected. Second, all connected patterns for the case of a finite grid cell, i.e. opposite grid cell borders are not connected, are identified. Third, for each border pair (north-south and east-west) it is tested if cells within a distance of  $R$  from both borders exists, that are part of a connected pattern for the infinite and finite grid cell case. If such a pattern exists than it is assumed to be infinite, because it loops around the grid cell surface of Lenia (Fig. 2, a). All other patterns are considered to be finite (Fig. 2, b). Please note that this method has a drawback. It can not identify certain infinite patterns that loop over several borders, for example, if a pattern exists that connects the north to east and then the west to south border (Fig. 3).

Moreover, there are two additional constraints that an animal pattern must fulfill. First, the cells of the connected pattern  $P = \{x_1, \dots, x_n\}$  must have at least 80% of all activation, i.e.  $\sum_{x \in P} A(x) \geq 0.8 \sum_{\forall y} A(y)$ . Second, a pattern must exist for the last two time steps ( $t = M$  and  $t = M - 1$ ). Both constraint are used to avoid that too small patterns or chaotic entities which change drastically between time steps are classified as animals. See Fig. 1, 23, 24, 25 and 26 for examples of animal patterns.

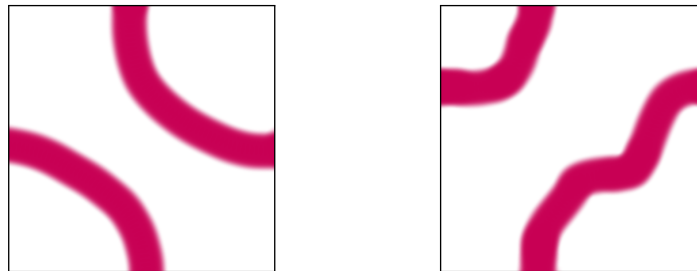


Figure 3: Examples of infinite patterns that are misclassified as a finite patterns.

**Non-Animal Classifier:** We also classified non-animal patterns which are all entities that were not dead and not an animal. These patterns spread usually over the whole state space and are connected via borders. See Fig. 23, 24, 25 and 26 for examples of non-animal patterns.

### 1.3 Statistical Measures for Lenia Patterns

We defined five statistical measurements for the final patterns  $A^{t=M}$  that emerge in Lenia. The measures were used as features for hand-defined goal spaces of IMGEPs and to define partly the analytic behavior space in which the results of the exploration experiments were compared.

**Activation mass  $M_A$ :** Measures the sum over the total activation of the final pattern and normalizes it according to the size of the Lenia grid:

$$M_A = \frac{1}{L^2} \sum_x A^{t=M}(x),$$

where  $L^2 = 256 \cdot 256$  is the number of cells of the Lenia system.

**Activation volume  $V_A$ :** Measures the number of active cells and normalizes it according to the size of the Lenia grid:

$$V_A = \frac{1}{L^2} |\{\forall x : A^{t=M}(x) > \epsilon\}| \text{ with } \epsilon = 10^{-4}.$$

**Activation density  $D_A$ :** Measures how dense the activation is distributed on average over all active cells:

$$D_A = \frac{M_A}{V_A}.$$

**Activation asymmetry  $A_A$ :** Measures how symmetrical the activation is distributed according to an axis that starts in the center of the patterns activation mass and goes along the last movement direction of this center. This measure was introduced to especially characterize animal patterns such as shown in Fig. 1. The center of the activity mass is usually also the center of the animals and analyzing the activity along their movement axis measures how symmetrical they are.

As a first step, the center of the activation mass is computed for every time step of the Lenia simulation and the Lenia pattern recentered to this location. This ensures that the center is all the time correctly computed in the case the animal moves and reaches one border to appear on the opposite border in the uncentered pattern. The center  $(\bar{x}, \bar{y})_t$  for time step  $t$  is calculated by:

$$(\bar{x}, \bar{y})_t = \left( \frac{M_{10}}{M_{00}}, \frac{M_{01}}{M_{00}} \right) \text{ with } M_{pq} = \sum_x \sum_y x^p y^q A^t(x, y),$$

where  $M_{pq}$  measures the image moment (or raw moment) of order  $(p + q)$  for  $p, q \in \mathbb{N}$ .

Based on the center  $(\bar{x}, \bar{y})_t$  the pattern  $A^t$  is recentered to  $A_C^t$  by shifting the  $x$  and  $y$  indexes according to the center:

$$A_C^t(x, y) = A^t((x - \bar{x}) \bmod L, (y - \bar{y}) \bmod L), \quad (2)$$

where  $L$  is width and length of the Lenia grid and the indexing is  $x, y = 0, \dots, L - 1$ . After each time step the center is recomputed and the pattern recentered:

$$A^{t=1} \xrightarrow{\text{recenter}} A_C^{t=1} \xrightarrow{\text{Lenia step}} A^{t=2} \xrightarrow{\text{recenter}} A_C^{t=2} \xrightarrow{\text{Lenia step}} \dots$$

Please note, the simulations and all figures of patterns in the paper are done with the uncentered pattern. The centered version is only computed for the purpose of statistical measurements.

The recenter step by  $(\bar{x}, \bar{y})_t$  defines also the movement direction of the activity center:

$$(m_x, m_y)_t = (\bar{x}, \bar{y})_t - (x^{\text{mid}}, y^{\text{mid}}) = (\bar{x} - x^{\text{mid}}, \bar{y} - y^{\text{mid}}),$$

where  $x^{\text{mid}}, y^{\text{mid}} = \frac{L-1}{2}$  are the coordinates for the middle point of the grid. A line can be defined that starts in the midpoint  $(x^{\text{mid}}, y^{\text{mid}})$  of the final centered pattern  $A_C^{t=M}$  and goes in and opposite to the final movement direction of the activity mass center  $(m_x, m_y)_{t=M}$ . This line separates the

grid in two equal areas. The asymmetry is computed by comparing the amount of activity in the grid right  $M_A^{right}$  and left  $M_A^{left}$  of the line. The normalized difference between both sides is the final asymmetry measure:

$$A_A = \frac{1}{M_A} (M_A^{right} - M_A^{left}).$$

**Activation centeredness  $C_A$ :** Measures how strong the activation is distributed around the activity mass center:

$$C_A = \frac{1}{M_A} \sum_x \sum_y w_{xy} \cdot A_C^{t=M}(x, y) \quad \text{with} \quad w_{xy} = \left(1 - \frac{d(x, y)}{\max_{y,x} d(x, y)}\right)^2,$$

where  $d(x, y) = \sqrt{(x - x^{\text{mid}})^2 + (y - y^{\text{mid}})^2}$  is the distance from the point  $(x, y)$  to the center point  $(x^{\text{mid}}, y^{\text{mid}})$ .  $A_C^{t=M}(x, y)$  is the centered activation that is updated every time step as for the asymmetry measure (Eq. 2). The weights  $w_{xy}$  decrease the farther a point is from the center. Thus, patterns that are concentrated around the center have a high value for  $C_A$  close to 1. Whereas, patterns whose activity is distributed throughout the whole grid have a smaller value. For patterns that are equally distributed ( $\forall_{x,x'} : A(x) = A(x')$ ) is  $C_A = 0$  defined as centeredness measure.

## 2 Sampling of Parameters for Lenia

All exploration algorithms explore Lenia patterns by sampling the parameters  $\theta$  that control Lenia. The parameters are comprised of the initial pattern  $A^{t=1}$  and the parameters which control the dynamic behavior ( $R, T, \mu, \sigma, \beta_1, \beta_2, \beta_3$ ). There are two operations to sample parameters: 1) random initialization and 2) mutating an existing parameter  $\theta$ . CPPNs are used for the random initialization and mutation of the initial pattern  $A^{t=1}$ . The details of this process are described in the next section. Afterwards, the initialization and mutation of Lenia’s parameter that control its dynamics are described.

### 2.1 Sampling of Start Patterns for Lenia via CPPNs

Compositional Pattern Producing Networks (CPPNs) are recurrent neural networks that were developed for the generation and evolution of gray-scale 2D images [15]. We used CPPNs to generate and mutate the initial state of Lenia  $A^{t=1}$  which resembles an image. CPPNs generate images pixel by pixel by taking as input a bias value, the  $x$  and  $y$  coordinate of the pixel in the image and its distance  $d$  to the image center (Fig. 4). Their output is the pixel value as a gray scale between 0 and 1 for the given  $(x, y)$  coordinate. For the generation of initial Lenia patterns is as input the  $x$  and  $y$  coordinate of the grid cells used. They were mapped to  $x = [-2, 2]$  and  $y = [-2, 2]$ . The distance to the grid center is given by  $d(x, y) = \sqrt{x^2 + y^2}$ . The final activity of a cell is the remapped output  $p$  of the CPPN via  $A(x, y) = 1 - |p|$ .

CPPNs consist of several hidden neurons (typically between 4 to 6 in our experiments) that can have recurrent connections and self connections. Each CPPN has one output neuron. Two activation functions were used for the hidden neurons and the output neuron. The first is Gaussian and the second is sigmoidal:

$$\text{gauss}(x) = 2 \exp(-2.5x^2) - 1, \quad (3)$$

$$\text{sigm}(x) = 2 \left( \frac{1}{1 + \exp(-5x)} \right) - 1. \quad (4)$$

To randomly initialize a Lenia initial pattern  $A^{t=1}$  a CPPN is randomly sampled by sampling the number of hidden neurons, the connections between inputs and neurons and neurons to neurons, their connection weights and the activation functions for neurons. Afterwards the initial pattern is generated by it. In the history  $\mathcal{H}$  of the IMGEPs is then the CPPN as part of the parameter  $\theta$  added. If the parameter is mutated, then the weights, connections and activation functions of the CPPN are mutated and the new initial pattern  $A^{t=1}$  generated by it. We used the *neat-python* package (<https://github.com/CodeReclaimers/neat-python>) for the random generation and mutation of CPPNs. It is based on the NeuroEvolution of Augmenting Topologies (NEAT) algorithm for the evolution of neural networks [16]. The meta-parameters for the initialization and mutation of CPPNs are listed in Table 1. The random sampling and mutation of CPPNs allows to generate complex patterns as illustrated in Fig. 5.

The random sampling of a new CPPN is done by the following steps. All CPPNs are initialized with 4 hidden neurons and 1 output neuron. Their activation functions are randomly assigned. Each

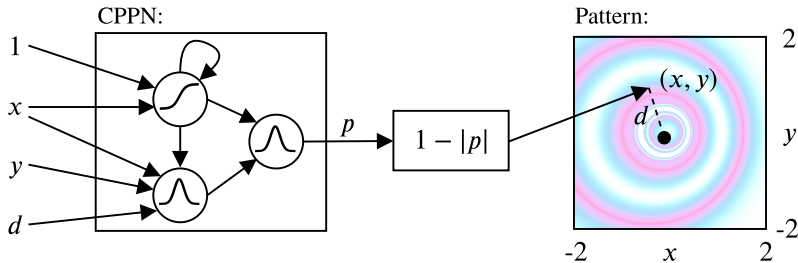


Figure 4: CPPNs are recurrent neural networks which take as input a bias of 1, the  $x$  and  $y$  coordinate of a point in the generated pattern and its distance  $r$  to the center of the pattern. Their output is the activity value of a grid cell.

Parameter	Value
Initial number of hidden neurons	4
Initial activation functions	gauss, sigm
Initial connections	random connections with probability 0.6
Initial synapse weight	Gaussian distribution with $\mu = 0, \sigma = 0.4$
Synapse weight range	$[-3, 3]$
Mutation neuron add probability	0.02
Mutation neuron delete probability	0.02
Mutation connection add probability	0.05
Mutation connection delete probability	0.01
Mutation rate of activation functions	0.1
Mutation rate of synapse weights	0.05
Mutation replace rate of synapse weights	0.06
Mutation power of synapse weights $\sigma_M$	1
Mutation enable/disable rate of synapse weights	0.02

Table 1: Configuration for the initialization and mutation of CPPN networks that generate the initial state for the Lenia system.

input-hidden, hidden-hidden and hidden-output neuron pair is connected with a probability of 0.6. The weights of each connection are sampled via a Gaussian distribution:  $w_{ij} \sim \mathcal{N}(\mu = 0, \sigma = 0.4)$ . The maximum and minimum weights for a connection are  $-3$  and  $3$ .

An existing CPPN is mutated by the following procedure. At first, structural mutations are performed. With probability 0.02 a new neuron  $z$  with a random activation function is added. The neuron is connected to the network by choosing randomly an existing connection. This connection is deleted. A connection from the source  $i$  of the deleted connection to the new neuron is added with weight  $w_{iz} = 1.0$ . Additionally, a new connection from the new neuron to the target  $j$  of the deleted connection is added with the old connection weight  $w_{zj} = w_{ij}$ , finishing the addition of a new neuron. With probability 0.02 one of the hidden neurons is deleted. With probability 0.05 a new connection is added between a random input-hidden, hidden-hidden or hidden-output neuron pair. The connection weight is sampled by the same method as for the sampling of new CPPNs. With probability 0.01 one random existing connection is removed. After the structural mutations the activation functions and weights are mutated. For each neuron the activation function is changed with probability 0.1 by randomly assigning a new activation function (either gauss or sigm). For each connection the weight is mutated by the following steps. With probability 0.05 the weight of the connection is changed according to:

$$w_{ij} \leftarrow [w_{ij} + \mathcal{N}(0, \sigma_M)]_{-3}^3 ,$$

where  $\sigma_M = 1$  is the mutation power and  $[n]_b^a = \min(\max(n, a), b)$  is the clip function. With probability 0.06 the connection weight is completely replaced by sampling a new one as done for the sampling of weights of new CPPNs.

Please note, the neat-python package allows also the setting and mutation of response and bias weights for each neuron. Those settings were not used for the experiments. Moreover, we adjusted the sigmoid and Gaussian function in the neat-python package to the ones defined in Eq. 3 and Eq. 4 to be able to replicate similar images as in [15].

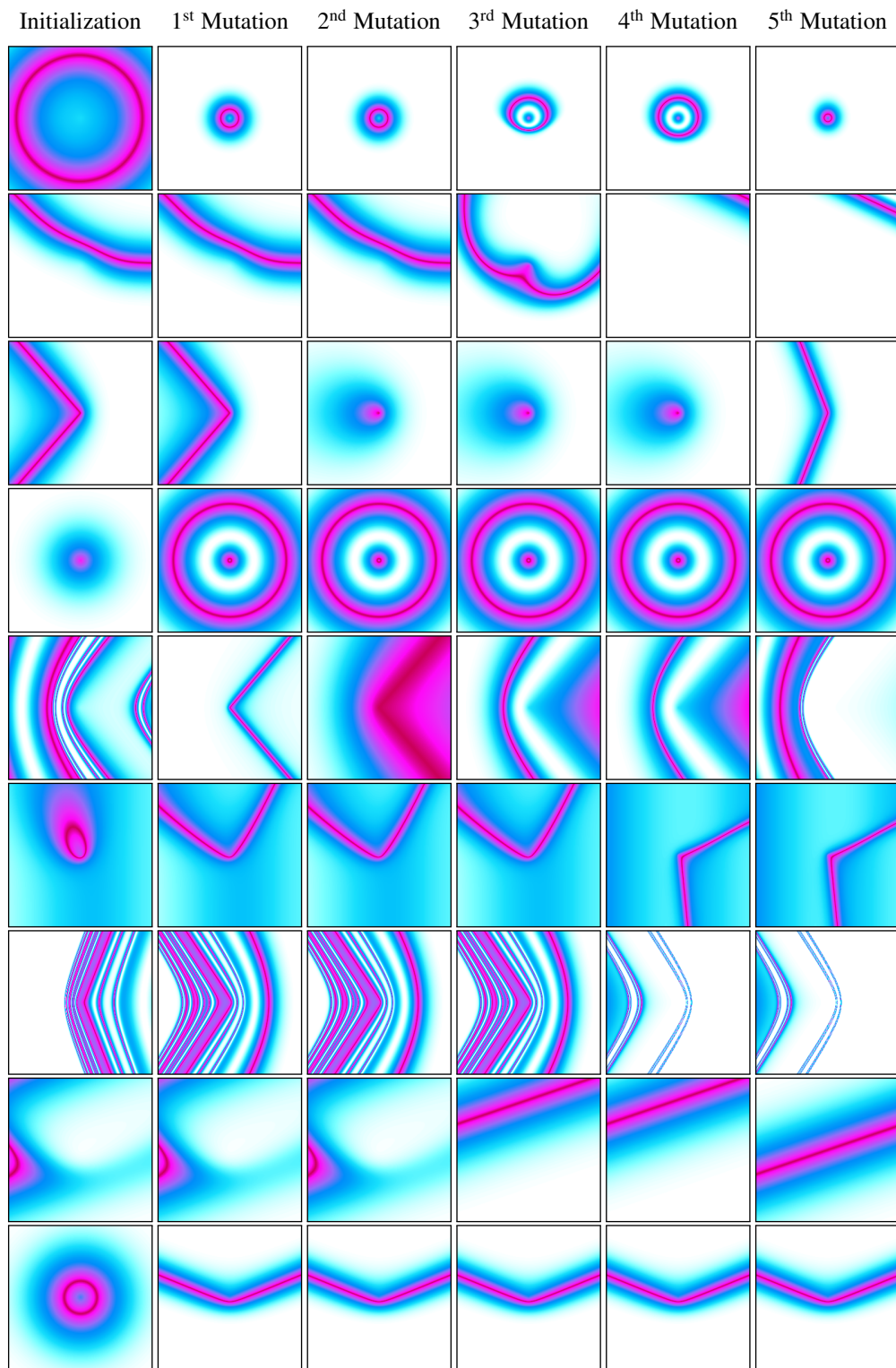


Figure 5: CPPNs can generate complex patterns via their random initialization and successive mutations. Each row shows generated patterns by one CPPN and its mutations.

## 2.2 Sampling of Lenia’s Dynamic Parameters

The parameters that control the dynamics of Lenia ( $R, T, \mu, \sigma, \beta_1, \beta_2, \beta_3$ ) are initialized and mutated via uniform and Gaussian distributions. Table 2 lists for each parameter the meta-parameters for their initialization and mutation. Each parameter is initialized by an uniform sampling  $\theta_i \sim \mathcal{U}(a, b)$  with  $a$  and  $b$  as upper and lower border. An existing parameter  $\theta_i$  is mutated by the following equation:

$$\theta_i \leftarrow [\theta_i + \mathcal{N}(0, \sigma_M)]_b^a,$$

where  $\sigma_M$  is the mutation power and  $[n]_b^a = \min(\max(n, a), b)$  is the clip function with  $a$  and  $b$  as upper and lower border. For natural numbers  $\theta_i \in \mathbb{N}$  the resulting value is rounded towards the nearest natural number.

Parameter	Type	Value Range	Mutation $\sigma_M$
$R$	$\mathbb{N}$	$[2, 20]$	0.5
$T$	$\mathbb{N}$	$[1, 20]$	0.5
$\mu$	$\mathbb{R}$	$[0, 1]$	0.05
$\sigma$	$\mathbb{R}$	$[0.001, 0.3]$	0.01
$\beta[1]$	$\mathbb{R}$	$[0, 1]$	0.05
$\beta[2]$	$\mathbb{R}$	$[0, 1]$	0.05
$\beta[3]$	$\mathbb{R}$	$[0, 1]$	0.05

Table 2: Settings for the initialization and mutation of Lenia system parameters  $\theta$ .

### 3 Measurement of Diversity in the Analytic Parameter and Behavior Space

The algorithms are compared on their ability to explore a diverse set of patterns. The next section introduces the diversity measure, followed by sections that introduce the spaces in which the algorithms are compared.

#### 3.1 Diversity Measure

Diversity is measured by the area that explored parameters cover in the parameter space of Lenia or that the identified patterns cover in the observation space. For the experiments the parameter space consisted of the initial start state of Lenia ( $A^{t=1} \in [0, 1]^{256 \times 256}$ ) and the settings for Lenia’s dynamics ( $R, T, \mu, \sigma, \beta_1, \beta_2, \beta_3$ ). The space consist therefore of  $256^2$  dimensions, each for a single grid cell of the initial pattern, plus 7 dimensions for the dynamic settings. The observation space consists of the final patterns  $A^{t=200} \in [0, 1]^{256 \times 256}$  resulting in  $256^2$  dimensions for the space. Each single exploration results in a new point in those spaces.

The diversity measures how much area the algorithms explored in those spaces (Fig. 6). The measurement is done by discretizing the space with a spatial grid and counting the number of discretized areas in which at least one point falls. For the discretization each dimension of the space is given a range, i.e. a minimum and maximum border. Each dimension is then split in a certain number of equally sized bins between those borders. The areas with values falling below the minimum or above the maximum border are counted as two additional bins.

The number of dimensions of the original parameter and observation space are too large to measure diversity in a meaningful manner. The initial pattern and the final pattern have  $256^2$  dimensions. We constructed therefore an analytic parameter and behavioral space where the latent representations of a  $\beta$ -VAE were used to reduce the high-dimensional patterns to 8 dimensions. The diversity in those spaces was compared between the algorithms. 5 bins (7 with the out of range values) per dimension were used for the discretization of those spaces for all experiments in the paper.

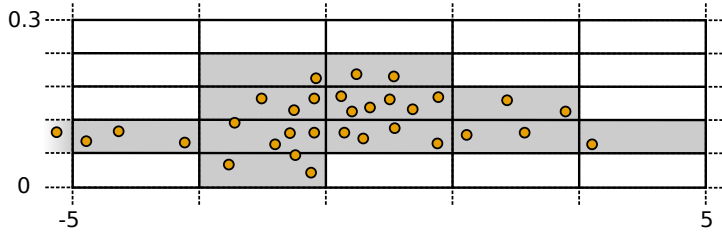


Figure 6: Illustration of the diversity measure in a two-dimensional space. The ranges for the dimensions were set to  $[-5, 5]$  and  $[0, 0.3]$ . The number bins per dimension is 5. Including the outlier areas the number of discretized bins is  $7^2 = 49$ . The diversity is the number of bins in which points exist (grey areas) which are 12 in this example.

#### 3.2 Analytic Parameter Space

The analytic parameter space was constructed by the 7 Lenia parameters that control its dynamics and 8 latent representation dimensions of a  $\beta$ -VAE (Table 3). The  $\beta$ -VAE was trained on initial patterns  $A^{t=1}$  used during the experiments. The dataset was constructed by randomly selecting 42500 patterns (37500 as training set, 5000 as validation set) from the experiments of all algorithms and each of their 10 repetitions. The  $\beta$ -VAE uses the same structure, hyper-parameters, loss function and learning algorithm as described in Section 5. It was trained for more than 1400 epochs with  $\beta = 5$  (Fig. 7). The encoder which resulted in the minimal validation set error during the training was used. According to its reconstructed patterns it can represent the general form of patterns but often not individual details such as their texture (Fig. 8).

#### 3.3 Analytic Behavior Space

The analytic behavior space was constructed by combining the 5 statistical measures for final Lenia patterns (Section 1.3) and 8 latent representation dimensions of a  $\beta$ -VAE (Table 4). The  $\beta$ -VAE

Analytic Parameter Space Definition					
Parameter	min	max	Parameter	min	max
R	1	20	$\beta$ -VAE latent 1	-5	5
T	2	10	$\beta$ -VAE latent 2	-5	5
$\mu$	0	1	$\beta$ -VAE latent 3	-5	5
$\sigma$	0	0.3	$\beta$ -VAE latent 4	-5	5
$\beta_1$	0	1	$\beta$ -VAE latent 5	-5	5
$\beta_2$	0	1	$\beta$ -VAE latent 6	-5	5
$\beta_3$	0	1	$\beta$ -VAE latent 7	-5	5
			$\beta$ -VAE latent 8	-5	5

Table 3: Features of the analytic parameter space and their min and max values

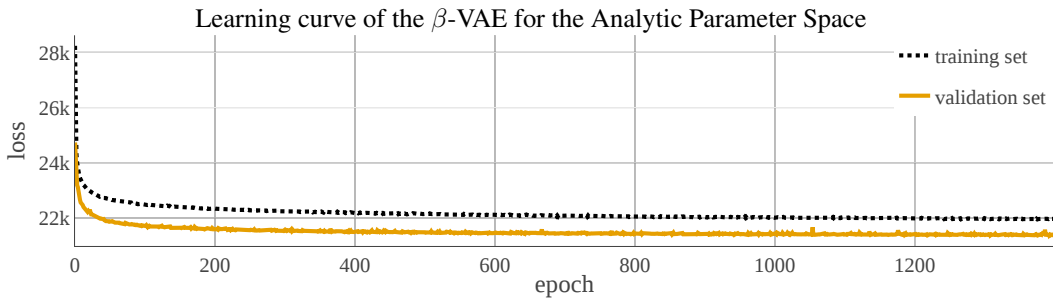


Figure 7: Learning curve of the  $\beta$ -VAE whose latent encoding was used for the analytic parameter space.

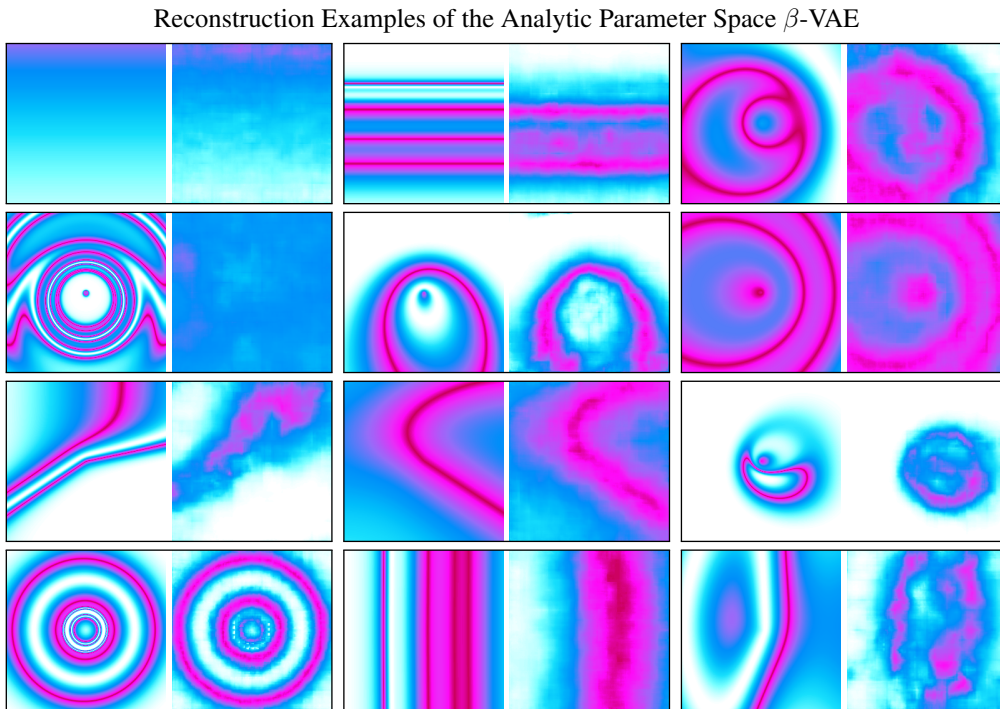


Figure 8: Examples of patterns (left) and their reconstructed output (right) by the  $\beta$ -VAE used for the construction of the analytic parameter space. The patterns are sampled from the validation dataset.

Analytic Parameter Space Definition					
Parameter	min	max	Parameter	min	max
mass $M_A$	0	1	$\beta$ -VAE latent 1	-5	5
volume $V_A$	0	1	$\beta$ -VAE latent 2	-5	5
density $D_A$	0	1	$\beta$ -VAE latent 3	-5	5
asymmetry $A_A$	-1	1	$\beta$ -VAE latent 4	-5	5
centeredness $C_A$	0	1	$\beta$ -VAE latent 5	-5	5
			$\beta$ -VAE latent 6	-5	5
			$\beta$ -VAE latent 7	-5	5
			$\beta$ -VAE latent 8	-5	5

Table 4: Features of the analytic behavior space and their min and max values

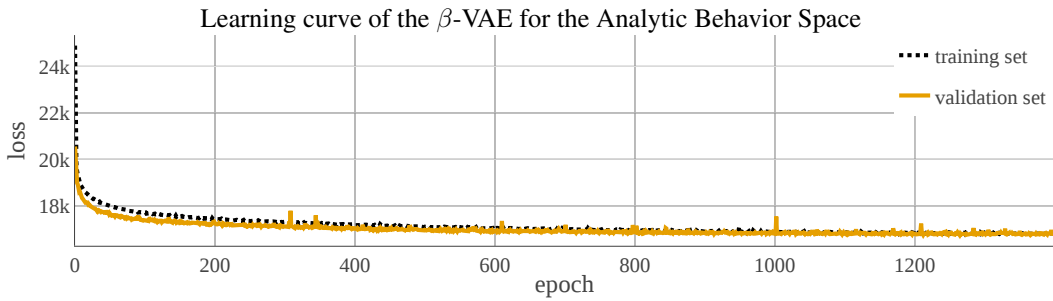


Figure 9: Learning curve of the  $\beta$ -VAE whose latent encoding was used for the analytic behavior space.

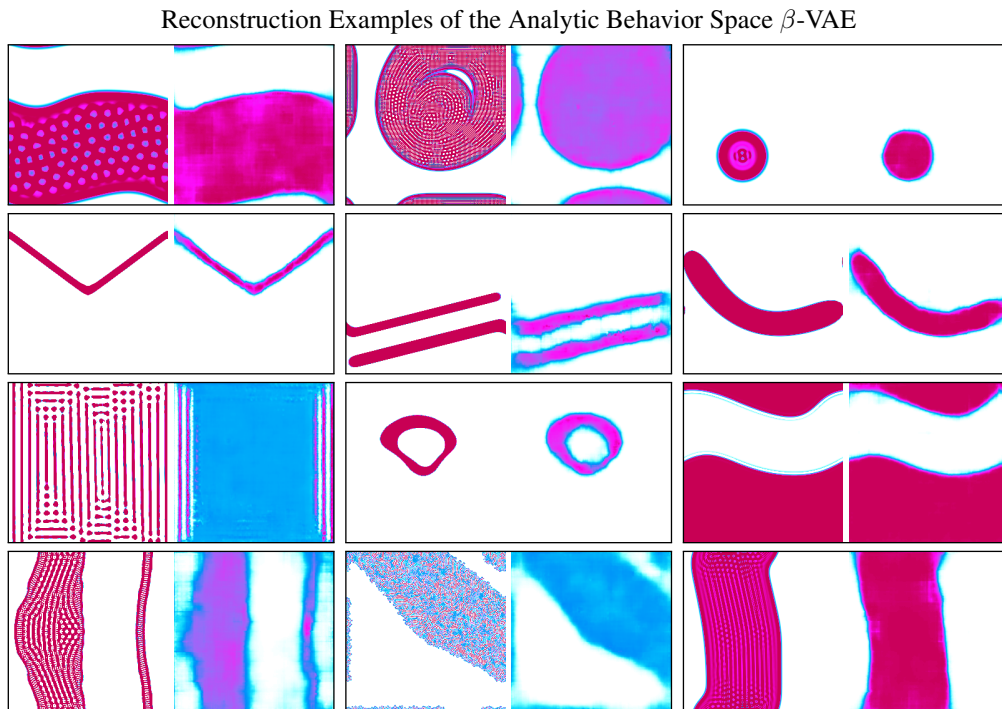


Figure 10: Examples of patterns (left) and their reconstructed output (right) by the  $\beta$ -VAE used for the construction of the analytic behavior space. The patterns are sampled from the validation dataset.

was trained on final patterns  $A^{t=200}$  observed during experiments. The dataset was constructed by randomly selecting 42500 patterns (37500 as training set, 5000 as validation set) from the experiments of all algorithms and each of their 10 repetitions. The dataset consists of 50% animal and 50% non-animal patterns. The  $\beta$ -VAE uses the same structure, hyper-parameters, loss function and learning algorithm as described in Section 5. It was trained for more than 1400 epochs with  $\beta = 5$  (Fig. 9). The encoder which resulted in the minimal validation set error during the training was used. Its reconstructed patterns show that it is able to represent the general form of patterns but often not individual details such as their texture (Fig. 10).

## 4 Random Exploration and IMGEPs with Hand-Defined Goal Spaces

Two random explorations and several IMGEPs with different hand-defined goal spaces were evaluated and compared. The main paper and the additional results in Section 6 only report the results for the best random exploration and one IMGEP variant with a hand-defined goal space. This section introduces the implementation details and diversity results of all evaluated random explorations and IMGEPs with hand-defined goal spaces.

### 4.1 Random Explorations

We evaluated two random exploration strategies: Random Initialization and Random Mutation. The main paper and the additional results in Section 6 only discuss the Random Initialization approach.

**Random Initialization:** This approach sampled for each of the 5000 explorations a random parameter  $\theta$  including a random CPPN to generate the initial state  $A^{t=1}$ . The approach can be replicated by using Algorithm 1 with  $N_{init} = 5000$ .

**Random Mutation:** This approach is closer to the principle of IMGEPs. It first performs  $N_{init} = 1000$  random explorations and adds each explored parameter  $\theta$  to a history  $\mathcal{H}$ . Afterwards, it randomly samples a parameter from the history and mutates it. The new parameter is also added to history  $\mathcal{H}$ . The approach can be replicated by using Algorithm 1 where line 6 is skipped and the parameter sampling distribution  $\Pi(g, \mathcal{H})$  is selecting a random parameter from the history and mutating it.

### 4.2 IMGEPs with Hand-Defined Goal Spaces

We evaluated several IMGEP variants with goal spaces that were hand-defined (IMGEP-HGS). Each space was constructed by a different combination of statistical measures of the final Lenia patterns (Tables 5 and 6) which are described in Section 1.3. The main paper and the additional results in Section 6 only discuss the IMGEP-HGS 9 approach. Algorithm 1 lists the steps of the IMGEP-HGS variants. They begin with  $N_{init} = 1000$  random explorations, followed by 4000 explorations based on randomly generated goals. Each goal was sampled from a uniform distribution within the ranges defined in Table 5. Then the parameter from a previous exploration that resulted in the closest outcome to the current goal was mutated and explored.

---

**Algorithm 1:** IMGEP-HGS

---

```
1 Initialize goal space representation  $\mathcal{R}$  by hand-defined features
2 for  $i \leftarrow 1$  to  $N$  do
3   if  $i < N_{init}$  then // Initial random iterations to populate  $\mathcal{H}$ 
4     Sample  $\theta \sim \mathcal{U}(\Theta)$ 
5   else // Intrinsically motivated iterations
6     Sample a goal  $g \sim \mathcal{G}(\mathcal{H})$  based on the space represented by  $\mathcal{R}$ 
7     Choose  $\theta \sim \Pi(g, \mathcal{H})$ 
8     Perform an experiment with  $\theta$  and observe  $o$ 
9     Append  $(o, \theta, \mathcal{R}(o))$  to the history  $\mathcal{H}$ 
```

---

### 4.3 Results

The random explorations and IMGEP-HGS variants are compared by their resulting diversity in the analytic parameter and behavior space (Fig. 11). The diversity is measured by the number of reached bins in each space using a binning of 7 bins per dimension.

The Random Initialization approach reached for all diversity measures a higher diversity than the Random Mutation approach. Therefore, the Random Initialization approach is used for the comparison to IMGEP approaches in the main paper and the additional results in Section 6.

Most IMGEP-HGS variants had a higher diversity in the analytic behavior space compared to random explorations, although their diversity in the analytic parameter space is lower. This shows the advantage of IMGEPs over random searches in discovering a wider range of patterns in the target

system. The best overall diversity had IMGEP-HGS 3, 4 and 9. We chose IMGEP-HGS 9 to compare it with learned goal spaces in the main paper and for the additional results in Section 6. It identified the highest diversity of non-animals of the three variants (3, 4, 9) reaching a higher diversity for non-animals than any IMGEP with a learned goal space. It was therefore selected to show that the choice of the goal space has an influence on the patterns that IMGEPs identify.

Depending on the statistical measures used to define the goal space the diversity between the IMGEP-HGS variants varied. IMGEPs that use the volume measure (HGS 1 - 4) reach in general a higher overall diversity which can be attributed to their higher diversity of animal patterns than goal spaces with the density measure (HGS 5 - 8) (Fig. 11, b, c). In terms of diversity of identified animals showed the inclusion of several measures the best performance (HGS 4 and HGS 8 in Fig. 11, c). In terms of diversity of identified non-animals showed the inclusion of several measures besides the centeredness  $C_A$  measure the best performance (HGS 3 and HGS 7 in Fig. 11, d). The results show that the choice of the goal space has an important influence on the diversity of identified patterns and their type (animal or non-animal).

Feature	min	max
mass $M_A$	0	1
volume $V_A$	0	1
density $D_A$	0	1
asymmetry $A_A$	-1	1
centeredness $C_A$	0	1

Table 5: HGS Goal Space Ranges

Feature	HGS-Variants								
	1	2	3	4	5	6	7	8	9
mass $M_A$	×	×	×	×	×	×	×	×	×
volume $V_A$	×	×	×	×					×
density $D_A$					×	×	×	×	×
centeredness $C_A$		×		×		×		×	×
asymmetry $A_A$			×	×			×	×	×

Table 6: IMGEP-HGS Variants

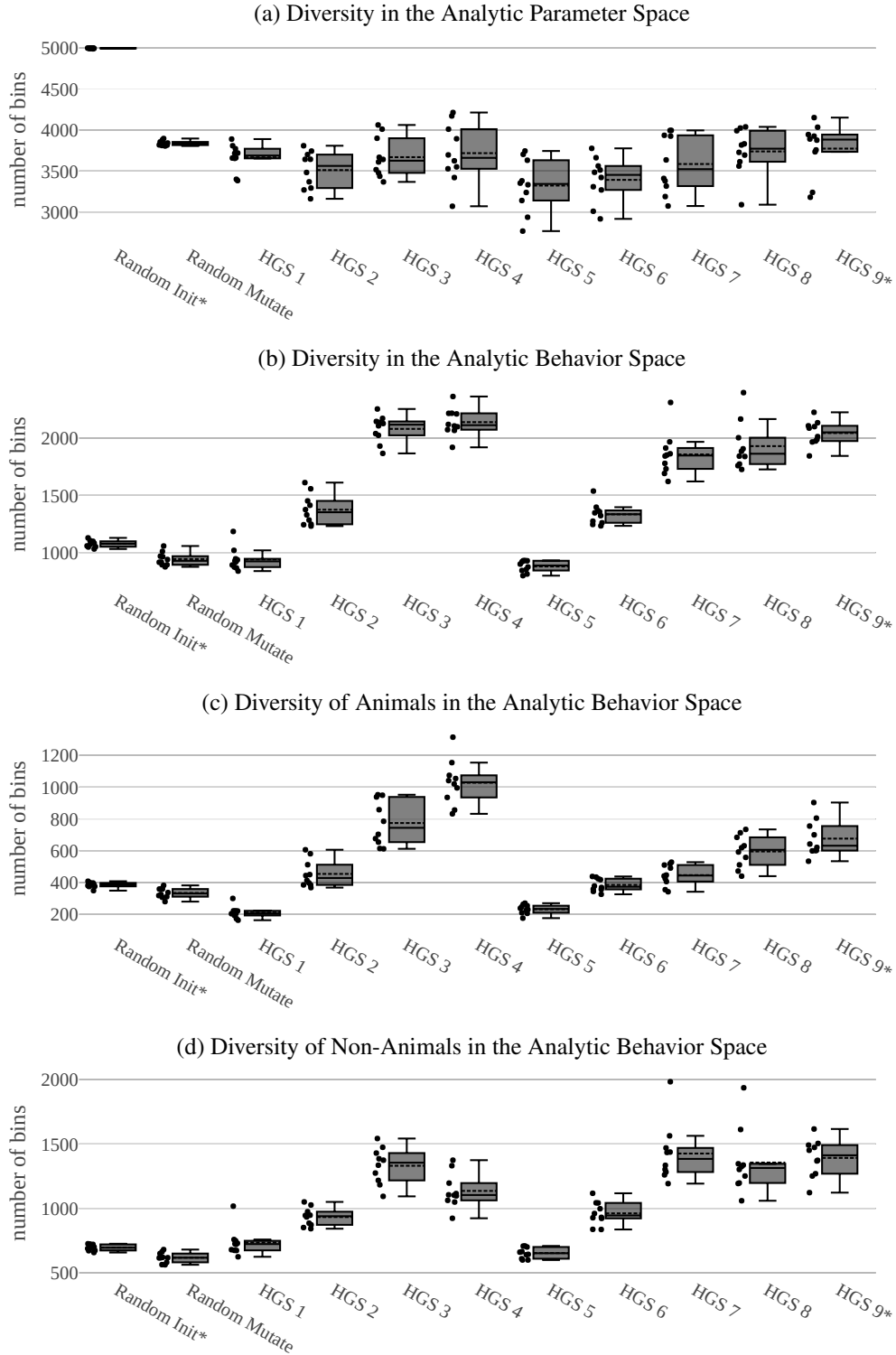


Figure 11: Although all IMGEP-HGS variants have lower diversity in the analytic parameter space compared to the Random Initialization approach, most of them have a higher diversity in the analytic behavior space. Each dot besides the boxplot shows the diversity of found patterns for each repetition ( $n = 10$ ). The box ranges from the upper to the lower quartile. The whiskers represent the upper and lower fence. The mean is indicated by the dashed line and the median by the solid line.

## 5 IMGEPs with Learned Goal Spaces via Deep Variational Autoencoders

For the IMGEPs using learned goal spaces (IMGEP-PGL and IMGEP-OGL) several deep VAEs were evaluated and compared. VAEs are artificial neural networks that learn a latent representation of data. The latent representation has a reduced number of dimensions and should capture the important features of the input data. We use VAEs to learn the important features that describe Lenia patterns. The features are then used to define goal spaces for IMGEPs. Section 5.1 explains the different variants that were implemented and Section 5.2 describes their implementation details.

### 5.1 VAE Variants

Variational Autoencoders (VAE) [10] have two components: a neural *encoder* and *decoder*. The encoder  $q(\mathbf{z}|\mathbf{x}, \chi)$  represents a given data point  $x$  in a latent representation  $\mathbf{z}$ . In variational approaches the encoder describes a data point by a representative distribution in the latent space of reduced dimension  $d$ . A standard Gaussian prior  $p(\mathbf{z}) = \mathcal{N}(0, I)$  and a diagonal Gaussian posterior  $q(\mathbf{z}|\mathbf{x}, \chi) = \mathcal{N}(\mu, \sigma)$  is used for this purpose. Given a data point  $x$ , the encoder outputs the mean  $\mu$  and variance  $\sigma$  of the representative distribution in the latent space. The decoder  $p(\mathbf{x}|\mathbf{z}, \psi)$  tries to reconstruct the original data  $x$  from a sampled latent representation  $\mathbf{z}$  for the distribution given by the encoder. Under these assumptions, training is done by maximizing the computationally tractable evidence lower bound (with  $\beta = 1$ ):

$$\mathcal{L}(\chi, \psi) = \underbrace{\mathbb{E}_{\mathbf{z} \sim q_{\chi}(\mathbf{z}|\mathbf{x})} [\log p_{\psi}(\mathbf{x}|\mathbf{z})]}_a - \beta \times \underbrace{\mathbb{D}_{KL}[q_{\chi}(\mathbf{z}|\mathbf{x}) \| p(\mathbf{z})]}_b . \quad (5)$$

The first term ( $a$ ) represents the expected reconstruction accuracy while the second ( $b$ ) is the KL divergence of the approximate posterior from the prior:

$$b = \mathbb{D}_{KL}[\mathcal{N}(\mu(\mathbf{x}), \Sigma(\mathbf{x})) \| \mathcal{N}(0, I)] = \sum_{i=1}^d \underbrace{\mathbb{D}_{KL}[\mathcal{N}(\mu(\mathbf{x})_i, \sigma(\mathbf{x})_i) \| \mathcal{N}(0, 1)]}_{b_i} . \quad (6)$$

Many current state-of-the-art approaches [3, 6, 8, 12] build on the VAE framework and augment the VAE objective to enhance interpretability and disentanglement of the latent variables. In this paper, we couple the VAE architecture with three different objectives: the classical VAE objective [10] (Equation (5) with  $\beta = 1$ ), the  $\beta$ -VAE objective [6] (Equation (5) with  $\beta > 1$ ) and an augmented  $\beta$ -VAE objective (Equation (7)).

The  $\beta$ -VAE objective re-weights the  $b$  term by a factor  $\beta > 1$ , aiming to enhance the disentangling properties of the learned latent factors. We are interested in such properties as it has been shown that it can benefit exploration [13]. However, heavily penalizing  $b$  can result in the network learning to “sacrifice” one or more of the learned latent variables in order to nullify their contribution  $b_i$  to this term (6). Those dimensions become completely uninformative and useless for further exploration in the learned latent space.

To prevent this phenomenon to happen, we augmented  $b$  with a new term that encourages the network to decrease *together* the individual contributions  $b_i$  of the different latent variables. This augmented loss term not only minimizes the averaged contribution (sum) but also the variance of the individual contributions:

$$b_{aug} = \sum_{i=1}^d b_i + \text{Var}([b_1, \dots, b_d]) . \quad (7)$$

Prior work also reports this phenomenon [1, 4, 5, 11, 17, 19] and other modifications of the training objective have been proposed [17, 19].

We tested the standard VAE,  $\beta$ -VAE and the augmented objective in the context of IMGEP to learn their goal spaces. The VAE networks were trained on the loss function given in Equation (8) with the hyper-parameters  $\{\beta = 1, \gamma = \mathbf{0}\}$ ,  $\{\beta = 5, \gamma = \mathbf{0}\}$  and  $\{\beta = 5, \gamma = \mathbf{1}\}$  corresponding to the three variants outlined above.

$$L = -a + \beta(b + \gamma \times c) \quad (8)$$

In the main paper paper, the results shown for the IMGEP-PGL and IMGEP-OGL approaches have been obtained with representations trained using the second variant ( $\beta$ -VAE objective). Its results were slightly better compared to the other VAE approaches, even though the results do not exhibit significant trends promoting one method over the other.

## 5.2 Implementation Details

This section describes the IMGEP approaches and the network architecture, training procedure, hyper-parameters and datasets for the training of their VAEs.

All VAEs use the same architecture (Table 7). The encoder network has as input the Lenia pattern and as outputs for each latent variable  $\mathbf{z}_i$  the mean  $\mu_i$  and log-variance  $\log(\sigma_i^2)$ . The decoder takes as input during the training for each latent variable a sampled value  $z_i \sim \mathcal{N}(\mu_i, \sigma_i^2)$ . For validation runs and the generation of all reconstructed patterns shown in figures the decoder takes the mean  $z_i = \mu_i$  as input. Its output is the reconstructed pattern.

The training objectives of all three variants are given in section 5.1. The resulting loss function (Eq. 8) of all VAE variants for a batch is:

$$\text{Loss}(x, \hat{x}, \mu, \sigma) = -a + \beta \left( \sum_{i=1}^d b_i + \gamma \text{Var}([b_1, \dots, b_d]) \right),$$

where  $x$  are the input patterns,  $\hat{x}$  are the reconstructed patterns,  $\mu, \sigma$  are the outputs of the decoder network and  $d$  is the number of latent dimensions. The reconstruction accuracy part  $a$  of the loss is given by a binary cross entropy with logits:

$$a = \frac{1}{N} \sum_{n=1}^N \sum_{j=1}^{L^2} (x_{j,n} \cdot \log \sigma(\hat{x}_{j,n}) + (1 - x_{j,n}) \cdot \log(1 - \sigma(\hat{x}_{j,n}))),$$

where the index  $j$  is for the single cells (pixel) of the pattern and  $n$  for the datapoint in the current batch,  $N$  is the batch size and  $\sigma(x) = \frac{1}{1+e^{-x}}$ . The KL divergence terms  $b_i$  are given by:

$$b_i = \frac{1}{2 \cdot N} \sum_{n=1}^N (\sigma_{i,n}^2 + \mu_{i,n}^2 - \log(\sigma_{i,n}^2) - 1).$$

All VAEs were trained for 2000 epochs. We used the Adam optimizer [9] ( $lr = 1e-3, \beta_1 = 0.9, \beta_2 = 0.999, \epsilon = 1e-8, \text{weight decay} = 1e-5$ ) with a batch size of 64.

The patterns from the datasets were augmented by random x and y translations (up to half the pattern size and with probability 0.3), rotation (up to 40 degrees and with probability 0.3), horizontal and vertical flipping (with probability 0.2). The translations and rotations were preceded by spherical padding to preserve Lenia spherical continuity.

Two types of IMGEPs were evaluated:

**IMGEP-PGL (prelearned goal space):** IMGEP (Algorithm 2) with a goal space defined by a VAE that was trained before the exploration starts. The VAE is trained on a dataset with precollected Lenia patterns. The best VAE model obtained during the training phase, i.e. the one with the highest accuracy on the validation data, is used for the exploration.

The dataset used to train the VAE has 558 patterns which are distributed into a training (75%), validation (10%) and testing (15%) datasets. Half of the patterns (279) were manually identified animal patterns by [2] (Fig. 1). The other half (279) are randomly initialized CPPN patterns as described in Section 2.1 (Fig. 5).

Encoder	Decoder
Input pattern A: $256 \times 256 \times 1$	Input latent vector $\mathbf{z}$ : $8 \times 1$
Conv layer: 32 kernels $4 \times 4$ , stride 2, 1-padding + ReLU	FC layers : $256 + \text{ReLU}, 16 \times 16 \times 32 + \text{ReLU}$
Conv layer: 32 kernels $4 \times 4$ , stride 2, 1-padding + ReLU	TransposeConv layer: 32 kernels $4 \times 4$ , stride 2, 1-padding + ReLU
Conv layer: 32 kernels $4 \times 4$ , stride 2, 1-padding + ReLU	TransposeConv layer: 32 kernels $4 \times 4$ , stride 2, 1-padding + ReLU
Conv layer: 32 kernels $4 \times 4$ , stride 2, 1-padding + ReLU	TransposeConv layer: 32 kernels $4 \times 4$ , stride 2, 1-padding + ReLU
FC layers : $256 + \text{ReLU}, 256 + \text{ReLU}, \text{FC}: 2 \times 8$	TransposeConv layer: 32 kernels $4 \times 4$ , stride 2, 1-padding

Table 7: VAE architecture for the pretrained and online experiments.

---

**Algorithm 2: IMGEP-PGL**

---

```
1 Initialize goal space encoder  $\mathcal{R}$  with the pretrained VAE
2 for  $i \leftarrow 1$  to  $N$  do
3   if  $i < N_{init}$  then // Initial random iterations to populate  $\mathcal{H}$ 
4     Sample  $\theta \sim \mathcal{U}(\Theta)$ 
5   else // Intrinsically motivated iterations
6     Sample a goal  $g \sim \mathcal{G}(\mathcal{H})$  based on space represented by  $\mathcal{R}$ 
7     Choose  $\theta \sim \Pi(g, \mathcal{H})$ 
8     Perform an experiment with  $\theta$  and observe  $o$ 
9     Append  $(o, \theta, \mathcal{R}(o))$  to the history  $\mathcal{H}$ 
```

---

**IMGEP-OGL (online learned goal space):** IMGEP (Algorithm 1 in the main paper) that trains the VAE which defines the goal space during the exploration. The VAE is trained on Lenia patterns discovered by the algorithm. Every  $K = 100$  explorations the VAE model is trained for 40 epochs resulting in 2000 epochs in total (less if there is not enough data after the first  $T$  runs to start the training).

Importance sampling is used to give the patterns in the training dataset a different weight during the training. A weighted random sampler is used that samples newly discovered patterns from the training dataset half of the time. Each pattern that has been added to the training dataset during the last period of 100 explorations has a probability of  $\frac{0.5}{N}$  to be sampled ( $N$  is the total number of new patterns in the dataset). Older patterns are also sampled half of the time each one with probability  $\frac{0.5}{|D_T| - N}$ . As a result, newer discovered patterns have a higher weight and a stronger influence on the training of the VAE model.

The datasets were constructed incrementally during the exploration by gathering non-dead patterns. One pattern every ten is added to the validation set (10%) and the rest is used in the training set. At the initial period of training, the training dataset amounts approximately 50 patterns and at the last period of training the dataset amounts approximately 3425 patterns (Fig. 12). The validation dataset only serves for checking purposes and has no influence on the learned goal space.

### 5.3 Results

We compared the different IMGEP variants (PGL and OGL) and VAEs (VAE,  $\beta$ -VAE and augmented  $\beta$ -VAE) with each other on the basis of the diversity of their identified patterns. Furthermore, the pattern reconstruction ability of the VAEs is analyzed.

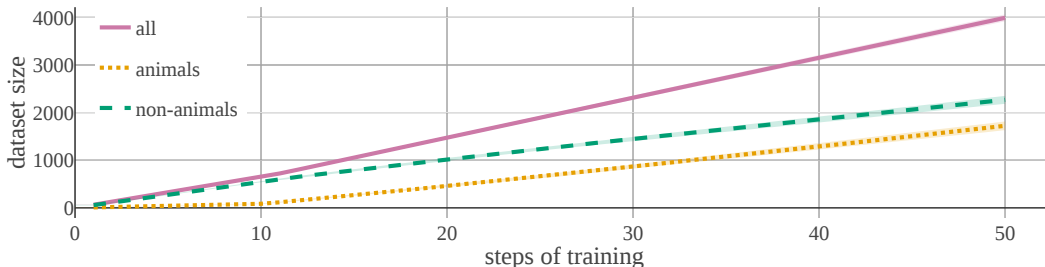


Figure 12: The IMGEP-OGL collects during the exploration animal and non-animal patterns to add them to its dataset for the training of the VAE. The figure shows the development of the averaged dataset size over all repetitions ( $n = 10$ ) of the IMGEP-OGL algorithm with a  $\beta$ -VAE. Standard deviation is depicted as a shaded area but for some not visible because it is too small.

### 5.3.1 Diversity

The algorithms are compared by their diversity in the analytic parameter and behavior space (Section 3). Diversity is measured by the number of discretized bins that were explored by the algorithms in each space if each dimension of the space is separated in 7 bins.

All IMGEP and VAE variants reached a higher diversity in the analytic behavior space compared to random explorations (Fig. 13, b), although random explorations have a higher diversity in the analytic parameter space (Fig. 13, a). This result confirms further the advantage of IMGEPs over random explorations in terms of identifying diverse patterns.

The difference between the PGL and OGL variants were small for all diversity measures. The OGL showed a slight advantage over the PGL versions in all diversity measures. Thus, an online version of the IMGEP can learn an appropriate goal space during the exploration. A precollected dataset as for the PGL is not necessary to successfully use IMGEPs.

The difference between the VAE variants (VAE,  $\beta$ -VAE and augmented  $\beta$ -VAE) was very small. The  $\beta$ -VAE was slightly better than the other two variants for the diversity in the analytic parameter space and for both IMGEP variants. All VAEs seemed to learn similar features for our datasets. It might be possible that the different VAE variants show different behaviors if their parameters are fine-tuned, such as the  $\beta$  parameter, but this was out of the scope of this paper. Because the  $\beta$ -VAE performed slightly the best, it was used for the results in the main paper and in Section 6.

### 5.3.2 VAE Pattern Reconstruction

All VAE variants showed a similar learning performance on the precollected dataset and the online collected dataset (Fig. 14 and 16). Their ability to reconstruct patterns based on the encoded latent representation is also qualitatively similar. For both datasets the VAEs are able to learn the general form of the activity pattern (Fig. 15 and 17). Nonetheless, the compression of the images to a 8-dimensional vector results in a general blurriness in the reconstructed patterns. As a result, the VAEs are not able to encode finer details and textures of patterns (Fig. 18). We believe this is the reason for their ability to identify more animals compared to the random exploration or the IMGEP-HGS. Different animals have often a different form, whereas non-animals span often over the whole area of Lenia's grid and differentiate mainly in their textures and small details. Because the VAE seem to encode more the general form a goal space based on them is more appropriate to find patterns with different forms such as the animals and not different textures which are important for non-animals.

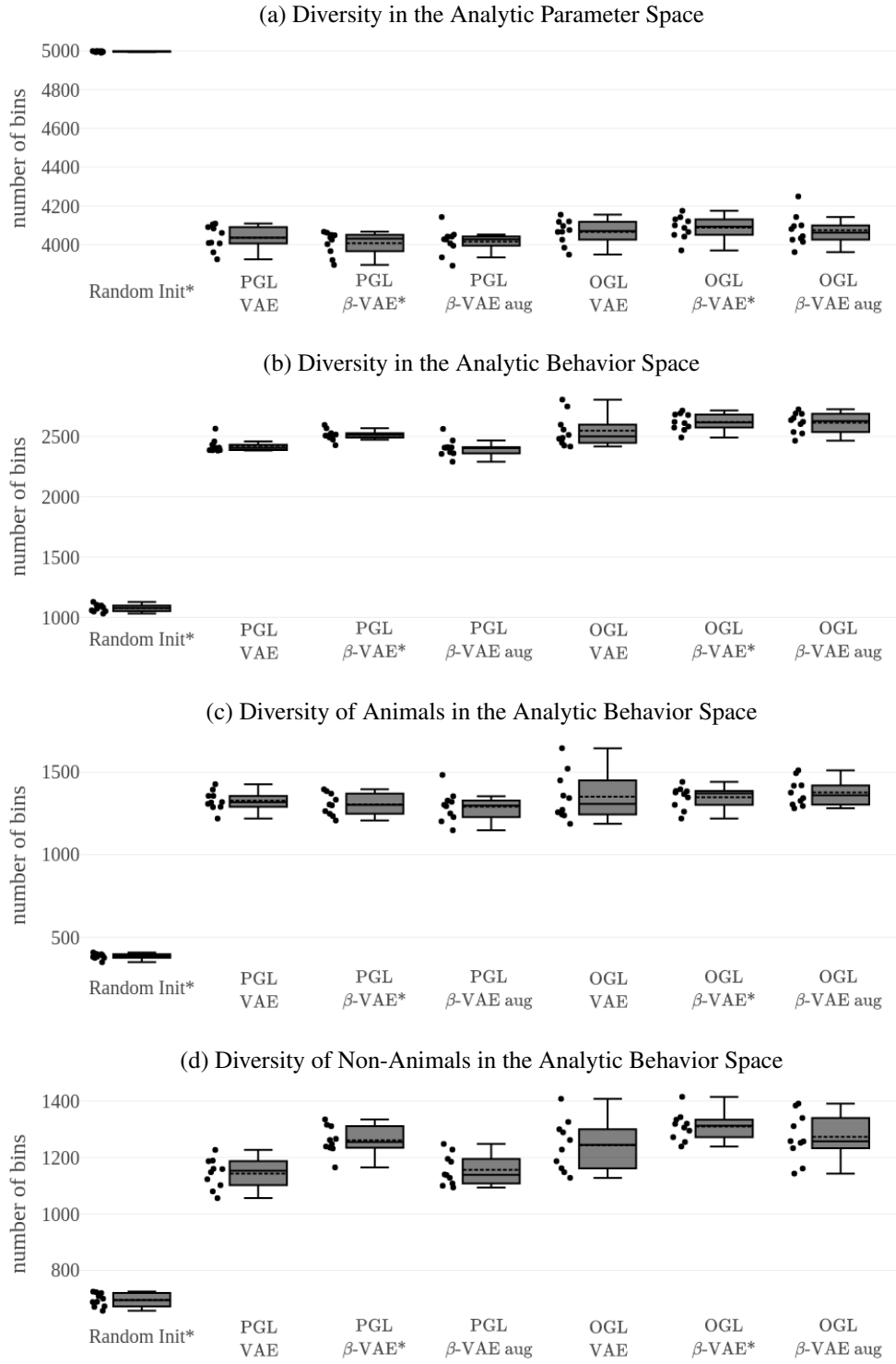


Figure 13: The different VAE algorithms showed only small differences in terms of diversity. The  $\beta$ -VAE had a slightly better diversity for the analytic behavior space for both IMGEP variants (PGL and OGL). Each dot besides the boxplot shows the diversity of found patterns for each repetition ( $n = 10$ ). The box ranges from the upper to the lower quartile. The whiskers represent the upper and lower fence. The mean is indicated by the dashed line and the median by the solid line.

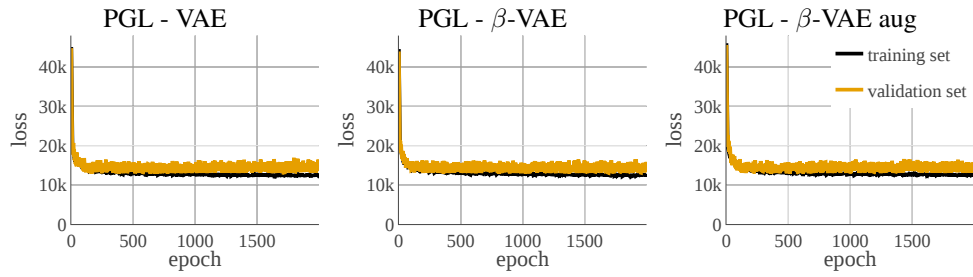


Figure 14: Averaged learning curves ( $n = 10$ ) of the VAEs for the IMGEP-PGL experiments.

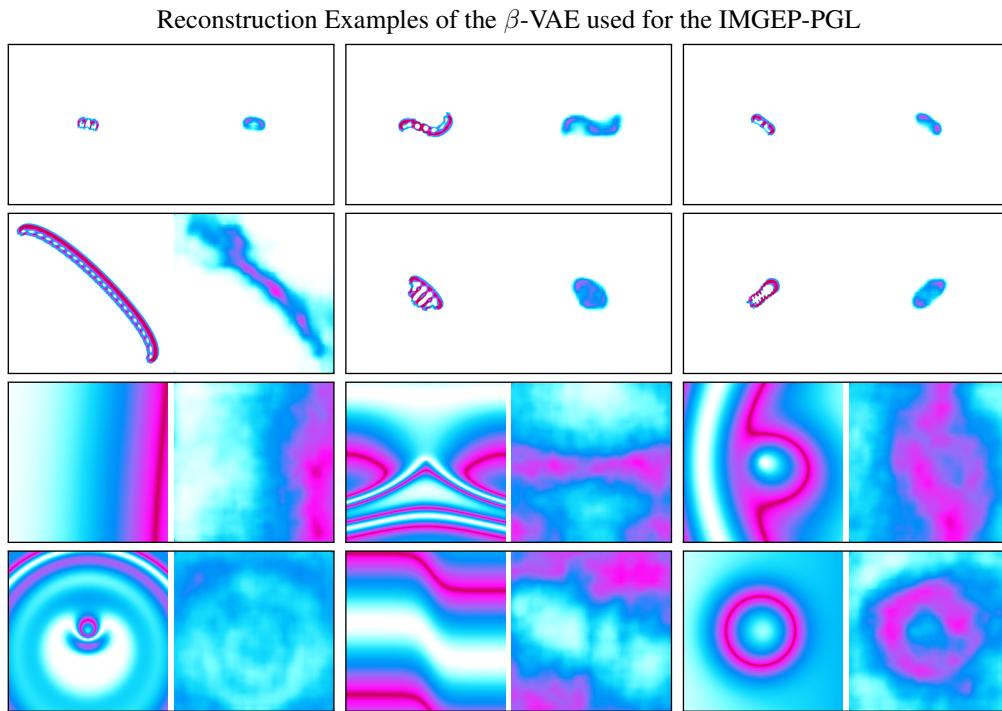


Figure 15: Examples of patterns (left) and their reconstructed output (right) by a VAE network used for the IMGEP-PGL. The patterns are sampled from its validation dataset. The dataset is composed of half animal patterns (rows 1 and 2) and half randomly generated CPPN patterns (rows 3 and 4).

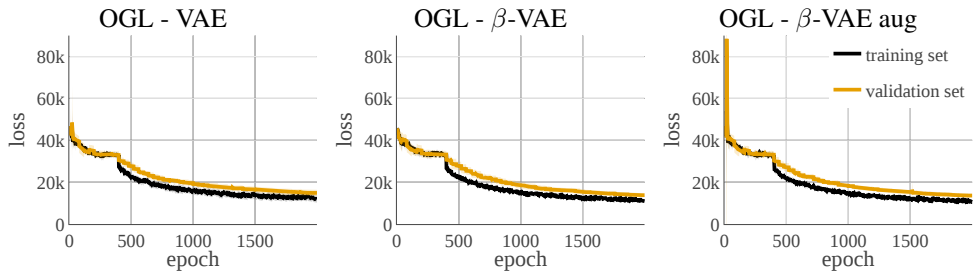


Figure 16: Averaged learning curves ( $n = 10$ ) of the VAEs for the IMGEP-OGL experiments.

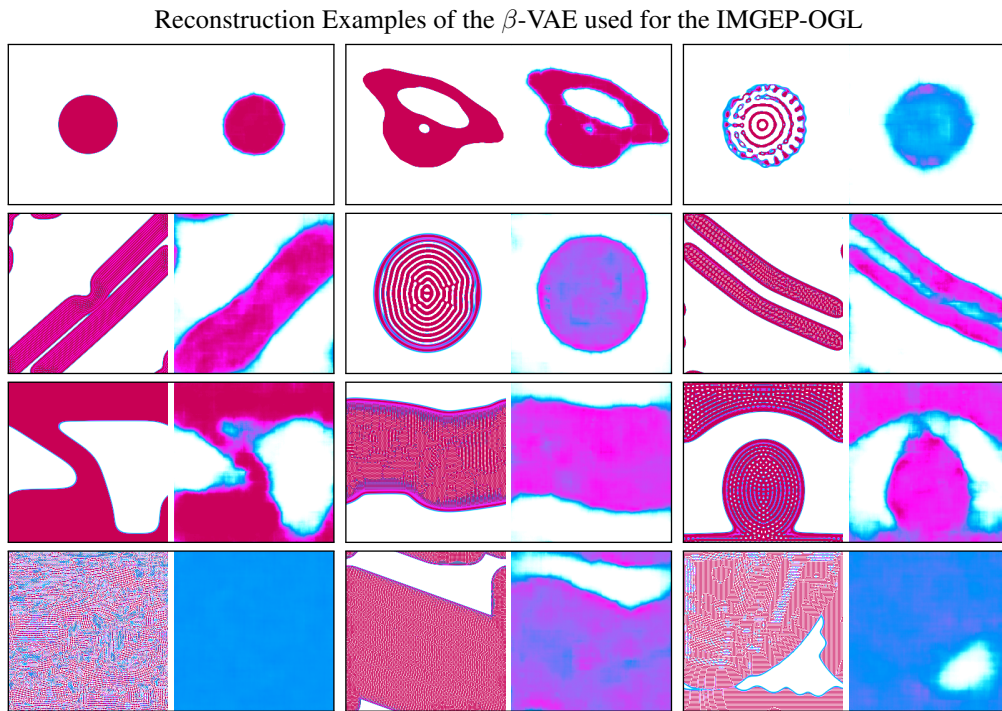


Figure 17: Examples of patterns (left) and their reconstructed output (right) by a VAE network used for the IMGEP-OGL. The patterns are sampled from its validation dataset. Animal patterns (rows 1 and 2) and non-animal patterns (rows 3 and 4) are shown.

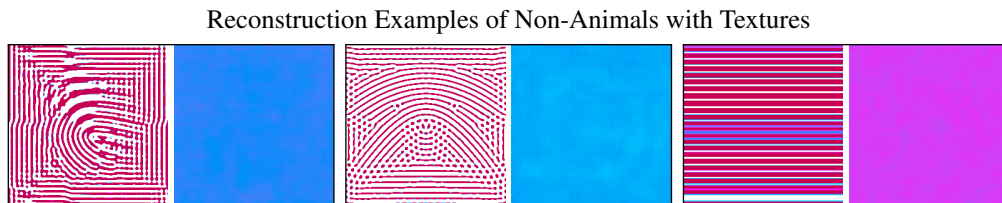


Figure 18: Examples of “textured” patterns that the VAE networks is unable to reconstruct. While a human eye can differentiate the input patterns (spatial frequency, orientation, etc.) the VAE reconstructs all images identically.

## 6 Additional Results

This section lists additional results. The results are only for a subset of all algorithm variants that have been evaluated. The results correspond to the following algorithms: Random to Random Initialization (Section 4), IMGEP-HGS to IMGEP-HGS 9 (Section 4), IMGEP-PGL to IMGEP-PGL with a  $\beta$ -VAE (Section 5) and IMGEP-OGL to IMGEP-OGL with a  $\beta$ -VAE (Section 5).

### 6.1 Number of Identified Patterns

The main paper used the measure of diversity of the found patterns per algorithm to compare their performance. Another measure to compare the algorithms is the number of the patterns they identified for each of the three pattern classes: dead, animals, non-animals (Fig. 19).

The results deviate slightly from the diversity measures. In terms of identified non-dead patterns outperform all IMGEP approaches a random exploration by finding between 10 to 20% more patterns. Although the IMGEP-HGS finds more non-dead patterns than the IMGEPs with learned goal spaces (OGL, PGL) its overall diversity in the analytic behavior space is smaller (Fig. 3, b of the main paper).

In the case the of animal patterns, all IMGEP approaches outperform the random exploration (8%). Within the IMGEP approaches the online learned goal space approach (IMGEP-OGL, 34%) and the pretrained goal space approach (IMGEP-PGL: 35%) find a similar amount. The hand-defined goal space approach identified less animal patterns (IMGEP-HGS: 19%). For non-animal patterns the hand-defined goal space approach identifies most patterns (IMGEP-PGL: 67%), followed by the random exploration (56%) and both learned goal space approaches (IMGEP-OGL: 45%, IMGEP-PGL: 43%). Although the number of identified non-animal patterns for the learned goal space approaches is low, their diversity is higher than for a random exploration and only slightly lower than for the hand-defined goal space approach (Fig. 3, d of the main paper).

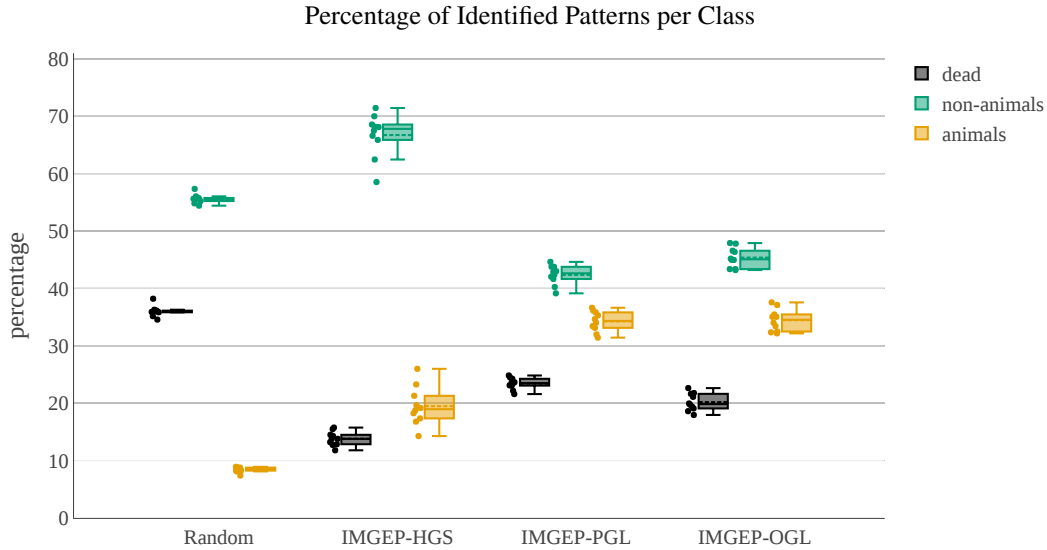


Figure 19: IMGEPs found more non-dead patterns compared to the random exploration. In terms of animals, the learned goal space approaches (IMGEP-PGL and OGL) found most animal patterns. For non-animals, the hand-defined goal space (IMGEP-HGS) found most patterns. The plot illustrates the percentage of found patterns for each class. Each dot besides the boxplot shows the percentage of found patterns for each repetition ( $n = 10$ ). The box ranges from the upper to the lower quartile. The whiskers represent the upper and lower fence. The mean is indicated by the dashed line and the median by the solid line.

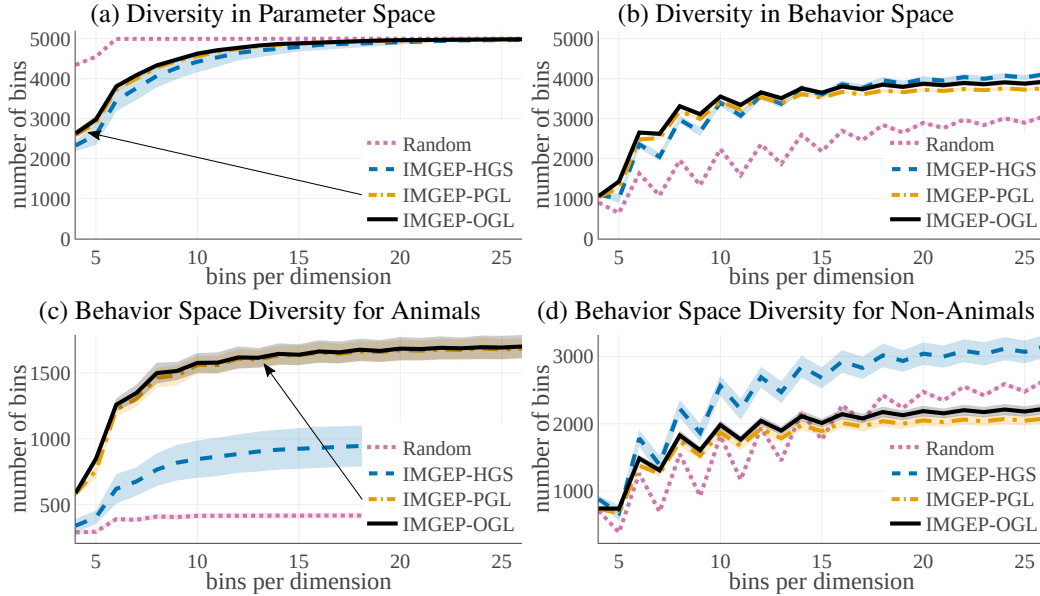


Figure 20: Dependencies of the diversity measure on the number of bins per dimensions for (a) the analytic parameter and (b-d) the behavior space. Depicted is the average diversity ( $n = 10$ ) with the standard deviation as shaded area (for some not visible because it is too small).

## 6.2 Dependence of the Diversity Measure on the Number of Bins per Dimension

The diversity of identified patterns measures the spread of the area which the identified patterns cover in the analytic behavior space (Fig. 3 in the main paper). The measure is defined by dividing the space in a number of discrete areas or bins (Section 3.1). The diversity is then measured by how many bins are covered during an exploration. The bins are created by dividing each dimension of the space into a number of equally-sized bins. We analyzed how the number of bins per dimension influences the diversity measure (Fig. 20).

Although the diversity difference between the algorithms depends on the number of bins per dimension for each space, the order of the algorithms, i.e. which algorithm has a higher diversity, is generally constant. Only if the number of bins per dimension grows large ( $> 10$ ) the order of the algorithms changes for some spaces and subpatterns. The order starts to follow the order seen for the number of identified patterns (compare the diversity with 25 bins per dimension in Fig. 20 with the number of identified patterns in Fig. 19). In this case the discretization of the space becomes too fine and each pattern falls into its own discretized area. We chose therefore a smaller number of bins per dimension of 7 (including the out of border bins) for all other diversity plots in the main paper and the Supplementary Material to compare the algorithms in a meaningful way.

## 6.3 Dimension Reduction of the Analytic Parameter and Behavior Space

A two-dimensional reduction of the identified patterns in the analytic parameter and behavior space (Section 3) visualizes the diversity of the parameters and identified patterns. The dimension reduction of the parameter space is based on all explored parameters encoded in the analytic parameter space from the first repetition experiment of all 4 algorithms. All encoded points were normalized so that the overall minimum value became 0 and the maximum value 1 for each dimension. Afterwards a principle component analysis (PCA) was performed to detect the 2 principle components [7]. The found patterns for each algorithm are plotted according to those components.

The results show that the random exploration has a stronger uniform distribution than any of the IMGEP algorithms in the analytic parameter space (Fig. 21). The IMGEP algorithms show concentrations of explorations in specific regions of the parameter space. The visualization shows also that it is not possible to define distinct regions in the parameter space that allow to differentiate between dead, animal and non-animal patterns.

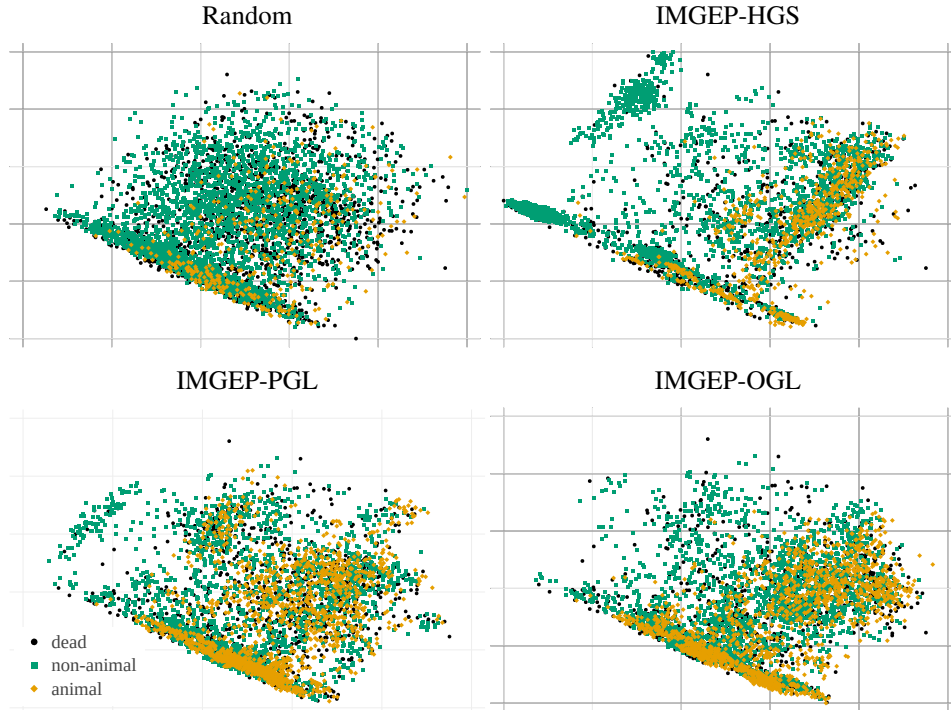


Figure 21: A random exploration covers the analytic parameter space more uniformly than IMGEP algorithms which form clusters at certain areas. PCA dimension reduction of the analytic parameter space which illustrates all explored parameters by the first repetition experiment per algorithm.

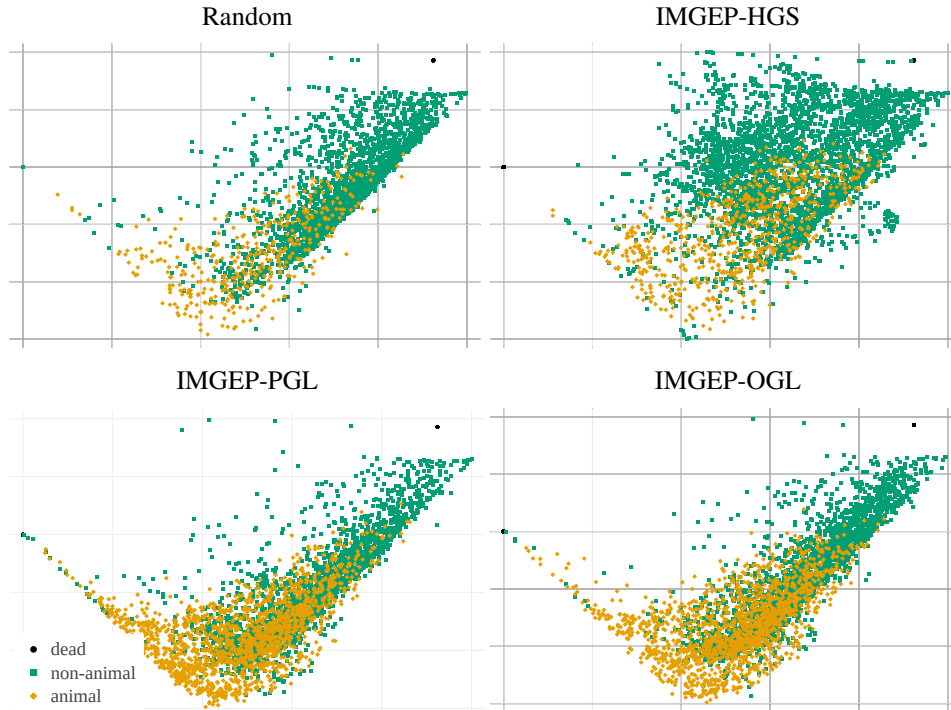


Figure 22: In the analytic behavior space IMGEPs reach a higher diversity compared to a random exploration. The HGS approach explores more non-animal areas and the PGL and OGL more animal areas. PCA dimension reduction of the analytic behavior space which illustrates all identified patterns by the first repetition experiment per algorithm.

The same analysis was performed for the identified patterns of each algorithm encoded in the analytic behavior space (Fig. 22). It is visible that the random exploration is more concentrated compared to the IMGEP approaches, especially in a region with many non-animal patterns (north-east). The IMGEP-HGS has a wider spread in the non-animal area. The IMGEPs with a learned goal space (PGL and OGL) show a stronger distribution in an area that encodes mostly animals (south).

#### 6.4 Identified Patterns

Fig. 23, 24, 25 and 26 illustrate examples of identified pattern per class (animal, non-animal, dead) and their ratio for the random exploration, IMGEP-HGS, IMGEP-PGL and IMGEP-OGL. The patterns have been randomly sampled from the results of the first exploration repetition experiment of each algorithm.

#### 6.5 Visualization of Goal Spaces

The goal space of IMGEPs is their most important element because it defines which type of patterns are set as goals for the exploration. This section provides complementary material for the analysis made in Section 5.2 of the main paper and shows further visualizations of goal spaces. The goal spaces of all IMGEP algorithms are visualized via a two-dimensional reduction of each goal space. Two techniques for dimensionality reduction were applied: PCA [7] and t-Distributed Stochastic Neighbor Embedding (t-SNE) [14].

The visualization was constructed by using for each exploration algorithm its goal space representations of all patterns it explored from a single repetition experiment. All goal representations were normalized so that the overall minimum value became 0 and the maximum value 1 for each goal space dimension. Afterwards the PCA was performed to detect the 2 principle components. T-SNE was executed by using the default standard Euclidean distance metric and default hyper-parameters (perplexity set to 50).

The resulting two-dimensional visualizations of the goal spaces make the differences between the algorithms visible (Fig. 27). For both approaches (PCA, t-SNE) has the hand-defined goal space (HGS) only a small area and a few clusters for animal patterns. In contrast, the learned goal spaces based on  $\beta$ -VAEs (PGL and OGL) have larger areas and more clusters for animal patterns. As a result, the learned goal spaces explore more animal patterns and find a higher diversity of them (Fig. 3, c) compared to the hand-defined goal space. The reason for this effect seems to be that the  $\beta$ -VAE which defines the goal space for the PGL and OGL is learning to represent the shape of patterns. The shape is an important feature of animals. Whereas, non-animals often cover the whole Lenia grid and differ mainly in their textures which the  $\beta$ -VAE does not represent well (Section 5).

The visualization serves as a support in qualitatively evaluating and comparing the efficiency of each algorithm in extracting a diversity of patterns from the data. Integrated into an interactive interface, these graphs are also useful for a potential human end-user to easily explore and visualize the different type of found patterns during the exploration phase. Videos and demonstrations of the interface can be found on the website <https://automated-discovery.github.io/>.



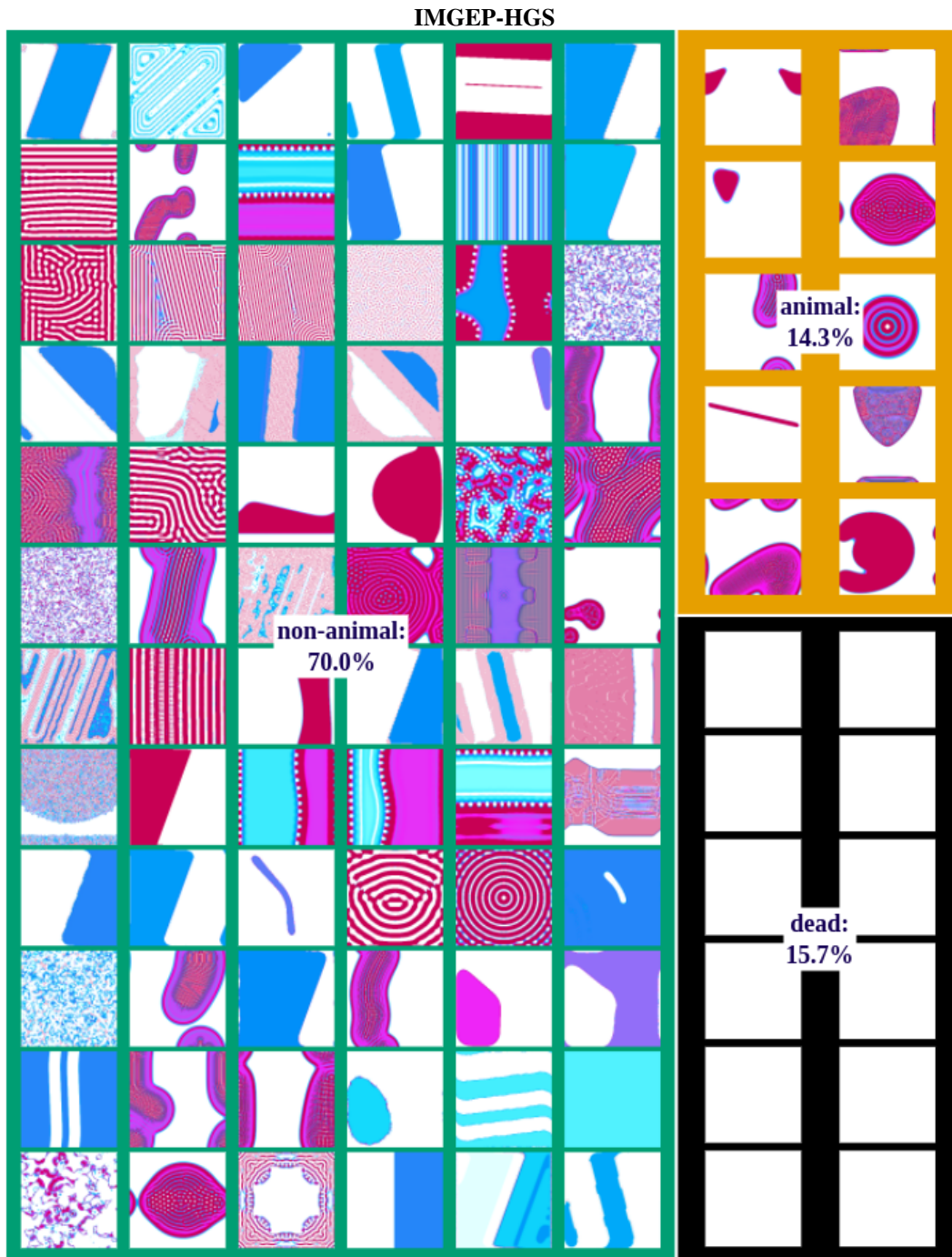


Figure 24: Examples of identified patterns for the IMGEP-HGS algorithm from the first repetition of experiments.

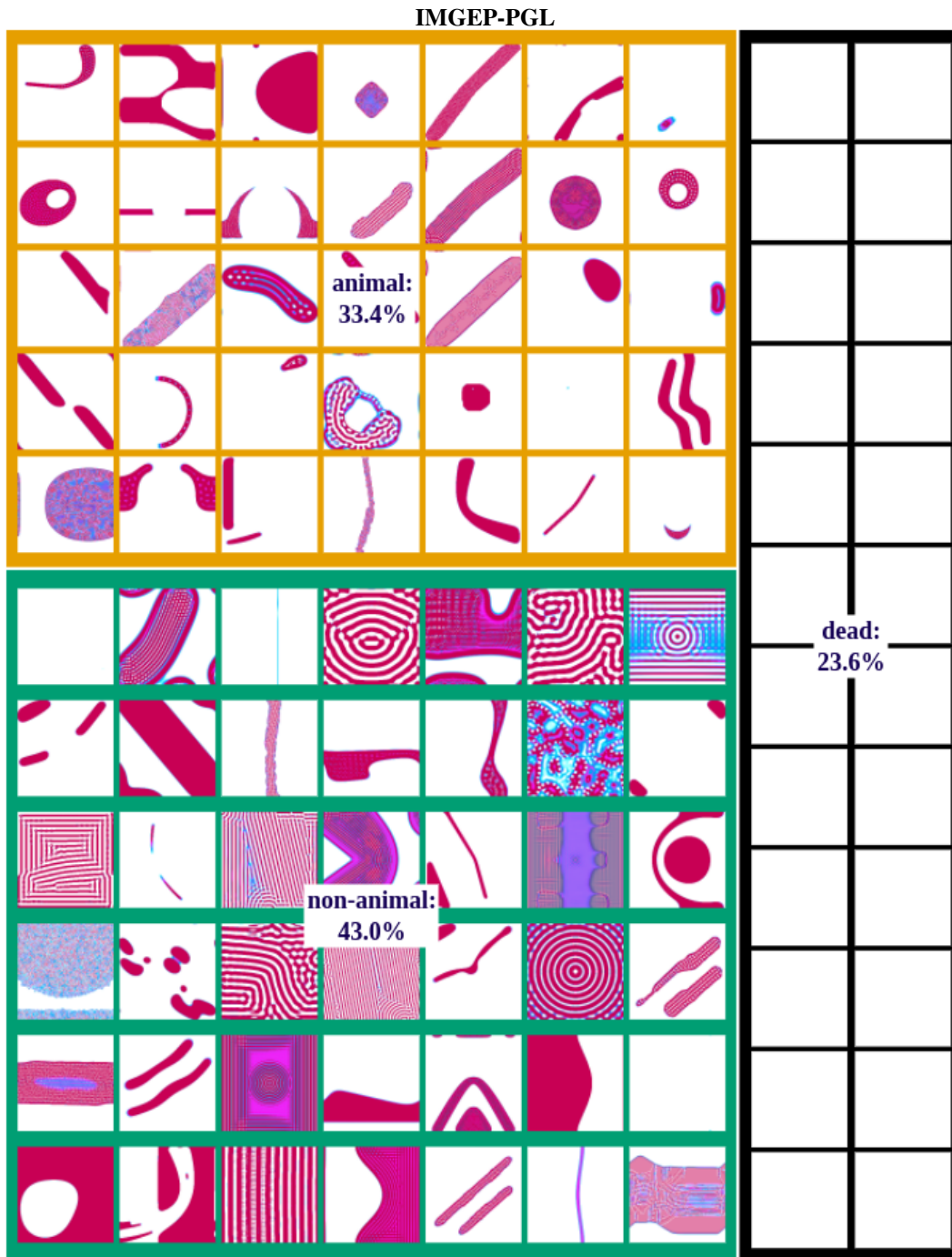


Figure 25: Examples of identified patterns for the IMGEP-PGL algorithm from the first repetition of experiments.

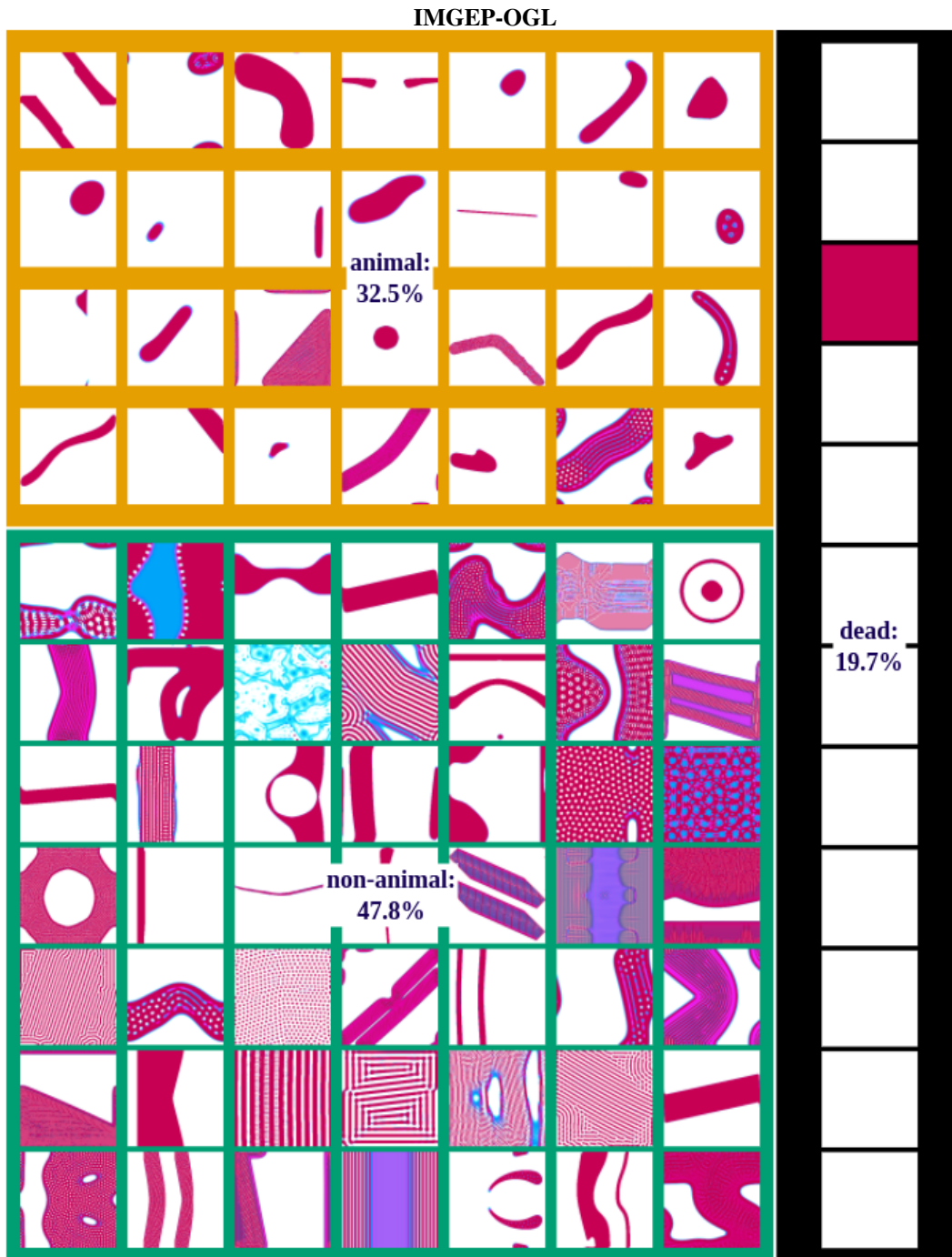


Figure 26: Examples of identified patterns for the IMGEP-OGL algorithm from the first repetition of experiments.

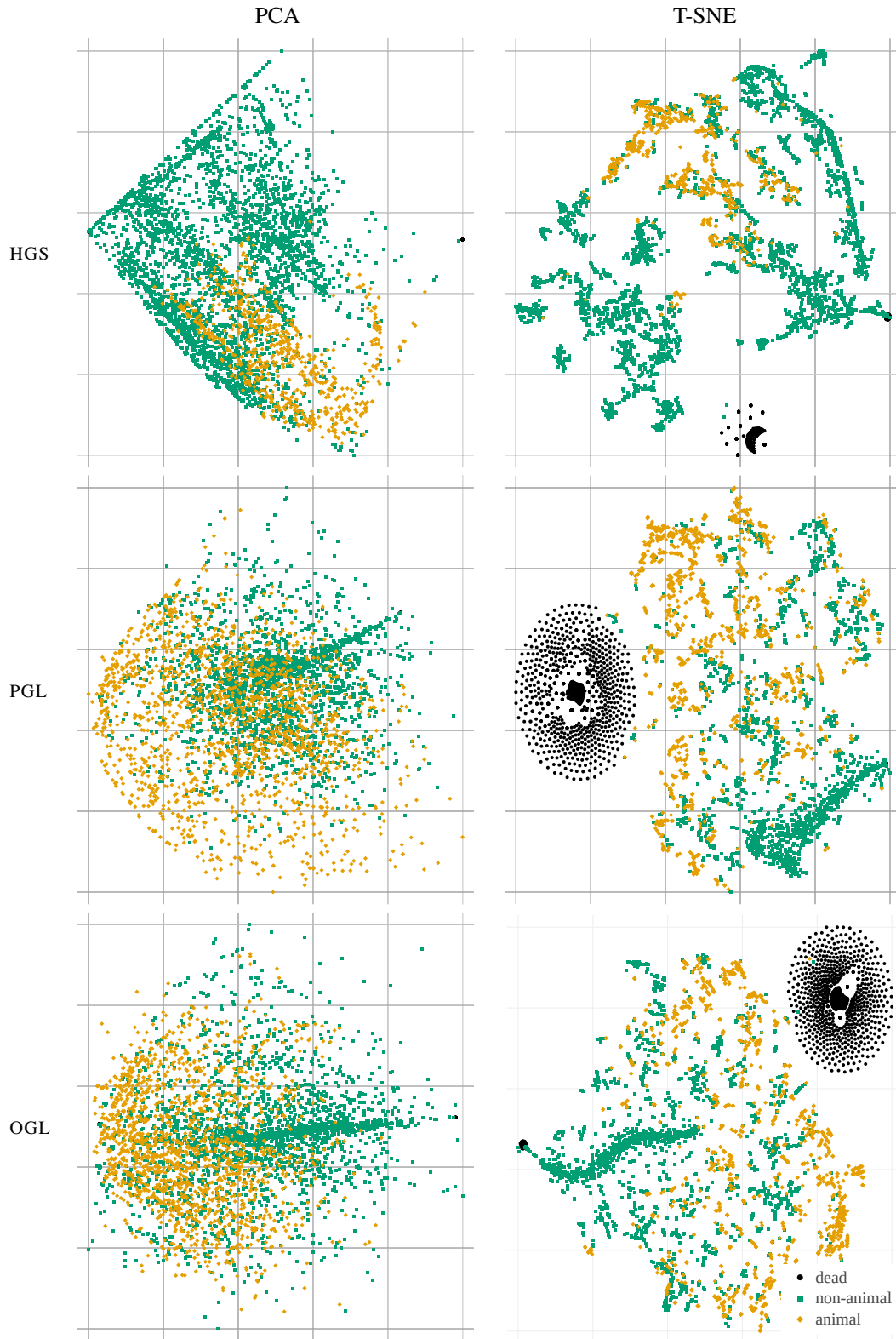


Figure 27: The PCA and t-SNE visualization of the goal spaces for the IMGEP variants shows that the hand-defined goal space (HGS) has more area and clusters for non-animals compared to learned goal spaces (PGL and OGL). They have more area and clusters for animals.

## References

- [1] Samuel R Bowman, Luke Vilnis, Oriol Vinyals, Andrew M Dai, Rafal Jozefowicz, and Samy Bengio. Generating sentences from a continuous space. *arXiv preprint arXiv:1511.06349*, 2015.
- [2] Bert Wang-Chak Chan. Lenia-biology of artificial life. *arXiv preprint arXiv:1812.05433*, 2018.
- [3] Tian Qi Chen, Xuechen Li, Roger B Grosse, and David K Duvenaud. Isolating sources of disentanglement in variational autoencoders. In *Advances in Neural Information Processing Systems*, pages 2610–2620, 2018.
- [4] Xi Chen, Diederik P Kingma, Tim Salimans, Yan Duan, Prafulla Dhariwal, John Schulman, Ilya Sutskever, and Pieter Abbeel. Variational lossy autoencoder. *arXiv preprint arXiv:1611.02731*, 2016.
- [5] Junxian He, Daniel Spokoyny, Graham Neubig, and Taylor Berg-Kirkpatrick. Lagging inference networks and posterior collapse in variational autoencoders. *arXiv preprint arXiv:1901.05534*, 2019.
- [6] Irina Higgins, Loic Matthey, Arka Pal, Christopher Burgess, Xavier Glorot, Matthew Botvinick, Shakir Mohamed, and Alexander Lerchner. beta-vae: Learning basic visual concepts with a constrained variational framework. In *International Conference on Learning Representations*, volume 3, 2017.
- [7] I. T. Jolliffe. *Principal Component Analysis and Factor Analysis*, pages 115–128. Springer New York, New York, NY, 1986.
- [8] Hyunjik Kim and Andriy Mnih. Disentangling by factorising. *arXiv preprint arXiv:1802.05983*, 2018.
- [9] Diederik P Kingma and Jimmy Ba. Adam: A method for stochastic optimization. *arXiv preprint arXiv:1412.6980*, 2014.
- [10] Diederik P Kingma and Max Welling. Auto-encoding variational bayes. *arXiv preprint arXiv:1312.6114*, 2013.
- [11] Durk P Kingma, Tim Salimans, Rafal Jozefowicz, Xi Chen, Ilya Sutskever, and Max Welling. Improved variational inference with inverse autoregressive flow. In *Advances in neural information processing systems*, pages 4743–4751, 2016.
- [12] Abhishek Kumar, Prasanna Sattigeri, and Avinash Balakrishnan. Variational inference of disentangled latent concepts from unlabeled observations. *arXiv preprint arXiv:1711.00848*, 2017.
- [13] Adrien Laversanne-Finot, Alexandre Pere, and Pierre-Yves Oudeyer. Curiosity driven exploration of learned disentangled goal spaces. In Aude Billard, Anca Dragan, Jan Peters, and Jun Morimoto, editors, *Proceedings of The 2nd Conference on Robot Learning*, volume 87 of *Proceedings of Machine Learning Research*, pages 487–504. PMLR, 29–31 Oct 2018.
- [14] Laurens van der Maaten and Geoffrey Hinton. Visualizing data using t-sne. *Journal of machine learning research*, 9(Nov):2579–2605, 2008.
- [15] Kenneth O Stanley. Exploiting regularity without development. In *Proceedings of the AAAI Fall Symposium on Developmental Systems*, page 37. AAAI Press Menlo Park, CA, 2006.
- [16] Kenneth O Stanley and Risto Miikkulainen. Efficient evolution of neural network topologies. In *Proceedings of the 2002 Congress on Evolutionary Computation.*, volume 2, pages 1757–1762. IEEE, 2002.
- [17] Ilya Tolstikhin, Olivier Bousquet, Sylvain Gelly, and Bernhard Schoelkopf. Wasserstein autoencoders. *arXiv preprint arXiv:1711.01558*, 2017.
- [18] Stephen Wolfram. Statistical mechanics of cellular automata. *Reviews of modern physics*, 55(3):601, 1983.
- [19] Shengjia Zhao, Jiaming Song, and Stefano Ermon. Infovae: Information maximizing variational autoencoders. *arXiv preprint arXiv:1706.02262*, 2017.